Journal of Hydrology: Regional Studies 56 (2024) 101954

Contents lists available at ScienceDirect

Journal of Hydrology: Regional Studies

journal homepage: www.elsevier.com/locate/ejrh

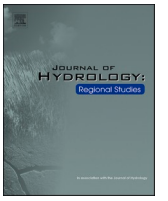

Spatial and temporal analysis and trends of extreme precipitation over the Mississippi River Basin, USA during 1988–2017

Atanas Dommo [a,b,c,d,*], Noel Aloysius [a,b,c,e,*], Anthony Lupo [b,c], Sherry Hunt [f]

[a] Department of Chemical and Biomedical Engineering, University of Missouri, Columbia, MO, USA
[b] School of Natural Resources, University of Missouri, Columbia, MO, USA
[c] Missouri Climate Center, University of Missouri, Columbia, MO, USA
[d] National Advanced School of Engineering, University of Yaounde 1, Yaounde, Cameroon
[e] Missouri Water Center, University of Missouri, Columbia, MO, USA
[f] Agroclimate and Hydraulics Engineering Research Unit, United States Department of Agriculture – Agricultural Research Service, Oklahoma and Central Plains Agricultural Research Center, Stillwater, OK, USA

ARTICLE INFO

Keywords:
Climate change
Extreme precipitation
Water management
Flooding
Droughts

ABSTRACT

Study region: Mississippi River Basin.
Study focus: Using daily precipitation records of 769 meteorological stations over the Mississippi River Basin (MRB), the spatial-temporal variability and trend of nine extreme precipitation indices were estimated and statistically assessed using the Mann-Kendall test. Factors likely to influence the spatial pattern and trends of precipitation extremes indices were also checked.
New hydrological insights for the region: The spatial pattern of the extreme precipitation indices exhibits a southeast to Northwest dipole, with the maximum values recorded over the south-eastern part of the domain (exception being for Consecutive Dry Days, CDD which shows otherwise) driven by the southerly moisture transport toward the southeast. The spatial pattern of the extreme precipitation is controlled by the topography. The results also show that, on average, almost all the indices (except CDD) exhibit an increasing trend. The total wet day precipitation exhibits a significant increasing trend. Spatially, most of the significant increasing (decreasing) trends of the extreme's precipitation-except CDD- are located over the Upper (South) MRB where there is a significant sign toward cooling (warming) conditions. This supports the view that changing climate towards warming (cooling) conditions is significantly affecting precipitations extremes over the MRB. The relationships between large-scale teleconnections and extreme precipitation show that Pacific North America significantly increases (decreases) frequency and intensity indices over the Northwest (southeast) MRB, whereas the Pacific Decadal Oscillation does increase the frequency and intensity indices over the southeast. El Niño Southern Oscillation significantly increases the frequency and intensity indices over the entire MRB, with consequences to infrastructure failures, increasing vulnerable populations, risk zones and relocations populations.

* Corresponding authors at: Department of Chemical and Biomedical Engineering, University of Missouri, Columbia, MO, USA.
E-mail addresses: dmmatanas@gmail.com, ad7gb@missouri.edu (A. Dommo), aloysiusn@missouri.edu (N. Aloysius).

https://doi.org/10.1016/j.ejrh.2024.101954
Received 3 January 2024; Received in revised form 12 August 2024; Accepted 27 August 2024
Available online 13 September 2024

1. Introduction

Precipitation is one of the important components of the hydrological cycle. In this era of changing climate, the stability of the global water cycle system has decreased (Yin et al., 2016) and precipitation is expected to change worldwide (Bessaklia et al., 2018; Gao et al., 2018). Furthermore, global warming has been shown to exacerbate and trigger variations in extreme precipitation (Xiong et al., 2009), which can result in droughts and floods, considerably impacting local environments, economies (Rosenzweig et al., 2002; Mantua et al., 2010) and ecosystems (Toreti and Desiato, 2008; Choi et al., 2009). Global changes of extreme climate variables observed in recent decades can only be accounted for by considering both anthropogenic and natural factors (Alexander et al., 2007). In some regions, both temperature and precipitation have already increased in response to changes in mean values (Smithson, 2002). It is widely conceived that as air temperature increases, the water cycling process will accelerate, but the consequences on the behavior of precipitation amount and intensity vary worldwide.

Throughout the U.S., many findings (Kunkel et al., 1999; Karl and Knight, 1998) claimed that the trend in short duration of extreme daily precipitation events has been increasing at a rate of 3–8 % per decade from 1931 to 1996. However, many studies (Balling and Goodrich, 2010; Peterson et al., 2013; Anderson et al., 2010, 2015; Griffiths and Bradley, 2007; Durkee et al., 2007; Brown et al., 2010; Howarth et al., 2019) relying only on the spatial-temporal analysis of the precipitation extreme indices across the U.S. mostly emphasize on the direction of trends with no further information regarding factors influencing the direction of the observed trends. Works from Anderson et al., (2015) have concluded that there is an increase in extreme precipitation frequency and intensity throughout the U.S. and since the last century (Hayhoe et al., 2018) with the increase in temperature alongside the increase in annual precipitation across most of the northern and eastern U.S. From a set of 774 weather stations spread over the U.S., Anderson et al., (2015) found positive trends in annual occurrence of rainfall across most of the U.S. and positive trends in annual intensity and heavy precipitation events across the Plains and Great Lakes. Karl et al., (1996) found and increasing in the number wet days over the U.S. much more than would be expected in a stationary climate between 1910 and 1940 and after 1970. However, some of the variability associated with changes in extreme precipitation events over the Eastern U.S. are related to changing patterns of large-scale tele-connections, such as the North Atlantic Oscillation (NAO), El Nino southern Oscillation (ENSO), and the Pacific North American pattern (PNA) (Griffiths and Bradley, 2007). In the same vein, Durkee at al., (2007) suggested that the statistically increasing trends in the frequency of extreme precipitation events observed over the eastern U.S. are associated with the positive phase of the NAO. Enfield et al., (2001) argued that the relationship between precipitation and Atlantic Multidecadal Oscillation (AMO) revealed an association

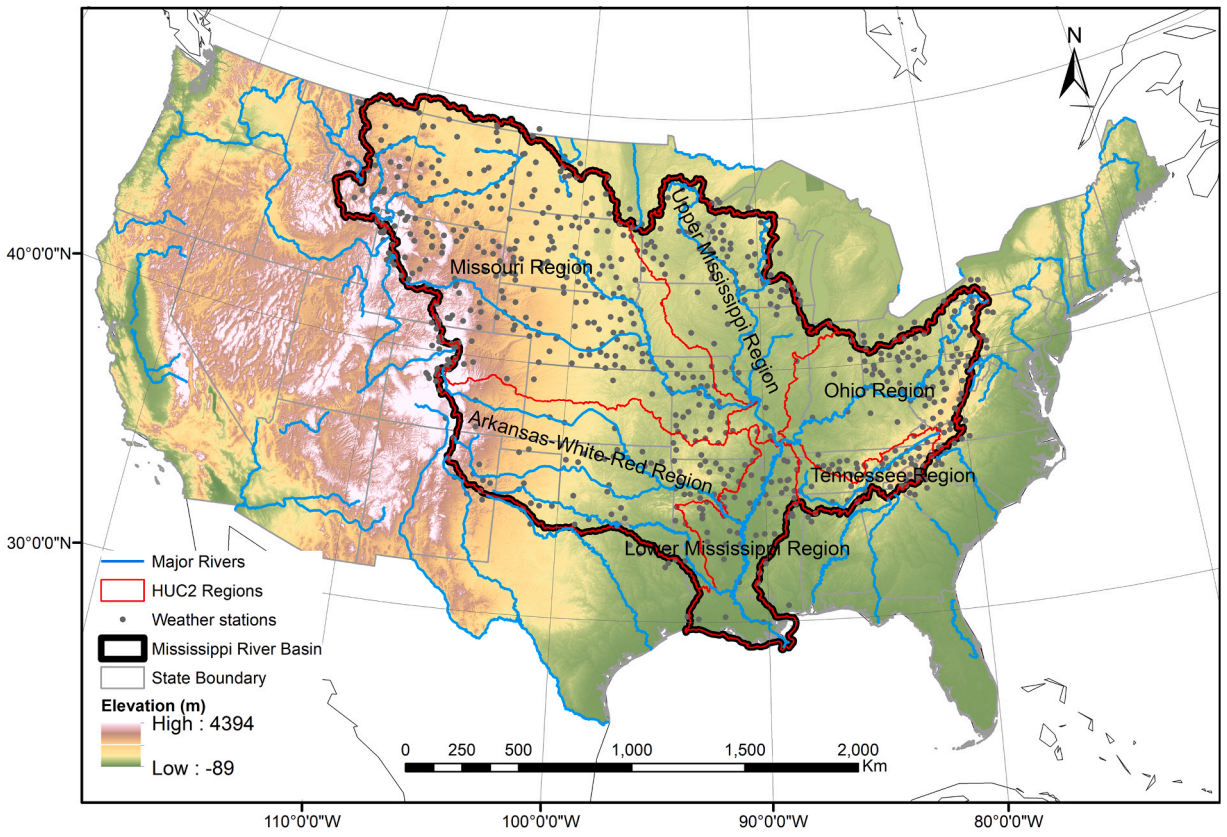

Fig. 1. Topography map of the study domain.

between the AMO warm phase with less than normal rainfall over the U.S., including Midwestern droughts. Similarly, Balling and Goodrich, (2010) attributed the spatial-temporal patterns and trend of precipitation intensity in the northeastern U.S. and center portion of the western U.S. to the influence of the AMO. Additionally, between AMO phases, the interannual pattern of rainfall is associated with ENSO, and the Mississippi River outflow varies by 10 % while the inflow to lake and Florida varies by 40 %. Curtis (2007) showed that the increase in precipitation intensity in Florida and over the Southeastern U.S. is linked to AMO warm phases. While the interannual fluctuations of rainfall are associated to ENSO, interdecadal fluctuations are associated to the Pacific Decal Oscillation (PDO) over the southern U.S. while Artic Oscillation (AO) have more impact over the Southeastern U.S. (Higgins et al., 2007). Maurer and Lettenmaier (2003) have shown the importance of ENSO and AO in the seasonal predictability of runoff over the Mississippi River Basin (MRB). Over the northeast U.S. (Howarth et al., 2019) a set of 58 weather stations were used to find that the increasing trend in extreme precipitation events during fall months is fed by tropical moisture leading to moisture surplus over 30 % of the country since 1970 (Karl et al., 1996). Most of those studies considered simple correlation as the tool to diagnose the relationship between extreme precipitation and large-scale teleconnections. Thus, these influences of large scale atmospheric and oceans teleconnections are worth considering -removing their mutual interaction to effectively quantify their individual impact- in any study related to possible causes of climate variability and their impacts on ecosystem functions and services. To the best of our knowledge, local factors likely to influence the spatial-pattern and the trends of extremes indices such as topography, the land use change (LUC) and the moisture haven't been documented enough in current literature. Understanding those factors is of paramount importance for local development and risk prevention. As the magnitude of global warming vary at regional and temporal scales, it is important to investigate the variability of extreme precipitation to address adequate responses for hazards and mitigate the negative impact on agriculture, ecosystems and the economy from a local to global scale.

Although many studies on extreme precipitation have already been conducted over different part of the U.S., few of those studies have paid particular attention to the spatial variability and trends of extreme precipitation over the MRB (Fig. 1). The MRB drains the third largest river in the world. The catchment (or drainage) area covers 41 % of the Conterminous U.S. and encompasses 31 states (Kesel et al., 1998, Fig. 1). Economically, the MRB is of national importance because of its significant agricultural and livestock production. The complex network of dams and levees help move most of the U.S. agricultural products originate from there (Foley et al., 2004). Nevertheless, the Mississippi River is vulnerable to river flooding, which occurs when the amount of runoff from the catchment area into a river exceeds the capacity of the channel (van der Wiel et al., 2018). Another cause of extreme flooding events in the MRB is the anomalously large water vapor transport from the Gulf of Mexico to the continental U.S. (Smith and Baeck, 2015; Benedict et al., 2019). In addition, the negative impacts of extreme precipitation events over the MRB are worth mentioning. For instance, many river-flooding with impact on agriculture and buildings, bridges, or dams in the Upper MRB (Wahl et al., 1993), Lower Mississippi and Ohio River Basins (Smith and Baeck, 2015) were the response to seasonal and longer extreme events and particularly from heavy precipitation.

Comprehensive analyses of factors such as moisture flux, topography and warming susceptible to influence the spatial structure and trends of extreme precipitation indices studied here are lacking in the current literature. The idea is to address climatic proxies that have a direct impact on infrastructure, agriculture, livestock, etc. To that end, the current study seeks to analyze the spatial-temporal variability of nine extreme's precipitation indices as defined by the Expert Team on Climate Change Detection and Indices (ETCCDI) (Table 1) over the MRB and investigate the factors likely to influence its variability. We hope that by doing so, we can enrich the current state of the knowledge on extreme precipitation over the MRB, identifying possible implications for better decision making. The paper is organized as follows: Section 2 describes the data and methods used in this study. The results of our findings are presented in Section 3. The discussion of our results is provided in Section 4 follow by the conclusion in Section 5.

Table 1
List of the nine climate indices used in this study.

Type	Indices	Name	Definition	Unit
Intensity indices	RX1day	Maximum 1-day precipitation amount	Maximum daily rainfall amount. Let RR*kj* be the daily rainfall amount on day *k* in the period *j*. The maximum daily values for the period *j* are: RX1day*j* = max (RR*kj*)	mm
	RX5day	Maximum consecutive 5-day precipitation amount	Maximum rainfall for 5-day interval. Let RR*kj* be the rainfall amount for the 5-day interval ending *k* in period *j*. The maximum 5-day values for the period *j* are: RX5day*j* = max (RR*kj*)	mm
	SDII	Simple daily intensity index	Average rainfall from wet days. Let RR*wj* be the daily rainfall amount on wet-day, PRCP $\geq$ 1 mm in period *j*. If *W* represents number of wet day in *j*, then: SDII*j* = total precipitation of wet for the period j divided by the number of wet days	mm/day
	PRCPTOT	Total wet days precipitation	Let RR_{ij} be the daily precipitation amount on day i in period *j*. PRCPTOT = sum of $RR_i \geq 1$ mm during the period *j*	mm
Frequency indices	R10mm	Number of heavy precipitation days	Let RR_{ij} be the daily precipitation amount on day i in period j. Count the number of days where $RR_{ij} \geq 10\ mm$	days
	R20mm	Number of very heavy precipitation days	Let RR_{ij} be the daily precipitation amount on day i in period j. Count the number of days where $RR_{ij} \geq 20\ mm$	days
	RR1	Number of wet days precipitation	counts of days when precipitation $\geq$1 mm	days
Duration indices	CDD	Consecutive dry days or dry spell	Maximum number of consecutive days with precipitation <1 mm	days
	CWD	Consecutive wet days or wet spell	Maximum number of days with precipitation $\geq$ 1 mm	days

2. Data and methods

2.1. Data

2.1.1. Precipitation gauge observations

Daily precipitation records were obtained from the National Oceanic and Atmospheric Agency (NOAA) Global Historical Climatology Network -Daily (GHCN-DAILY) database for the period of 1988–2017 (Menne et al., 2012). This database was designed to fulfill the need for daily climate data around the world and for the wide variety of applications including climate analysis and monitoring studies. Quality control checks are routinely applied to the dataset to avoid inconsistency in the data timeseries. We retrieved the daily data at 1240 locations within the study area (see Fig. 1 for locations). The daily data come from at least 12 databases as described in Menne et al., (2012, see their Table 2). No attempts were made to fill the missing values. To ensure the quality of the analyses and consider a daily precipitation timeseries as complete, we first consider stations that record at least 95 % of data (Klein Tank and Können, 2003) per year for the period 1988–2017. Then, with the aim of detecting inhomogeneous series, three homogeneity tests were applied to the weather stations' precipitations time series, namely the Standard Normal Homogeneity Test (SNHT) (Alexandersson, 1986), Buishand Range Test (Buishand, 1982), and Pettitt Test (Pettitt, 1979). These homogeneity tests are based on different statistical principles. They are therefore complementary and have the advantage of being able to detect inhomogeneity at different levels of the precipitation time series. Only the stations that passed the three-homogeneity tests were considered. In summary, for a total of 1240 stations, 769 stations were chosen for the continuity and the homogeneity of their data records during the period of 1988–2017.

2.1.2. Atmospheric and oceanic teleconnections index

Large-scale teleconnection patterns may influence many facets of precipitation in weather stations (Cullen and deMenocal, 2000; Donat et al., 2013; Trenberth et al., 2003). These teleconnections impact rainfall patterns through the changing of the planetary wave in a various times scale. Those teleconnections include ENSO (Higgins et al., 2007) with impact on interannual fluctuations of precipitations, while PDO and AO may play a major role in decadal or interdecadal fluctuation on rainfall intensity. Several authors (Bradley, 2007; Durkee et al., 2007) have also investigated the impact of Pacific North American (PNA), AO and AMO on precipitation intensity. This study utilizes seven large teleconnections index including: (1) the unsmoothed and detrended AMO index (Enfield et al., 2001); (2) the PNA index, which is known as a natural mode of climate variability and is one of the most important modes of low frequency variability in the Northern hemisphere extra tropics; (3) the ENSO index, which is computed by removing the mean to the area averaged sea surface temperature (SST) from 5S-5 N & 170–120 W (Rayner et al., 2003); (4) the AO index (Thompson and Wallace, 1998; 2001), which is known as a large scale mode of climate variability and also referred to as the northern hemisphere annular mode, has a wide range of influences on weather in north America and is characterized by opposing fluctuations in barometric pressure over the polar region and midlatitudes; (5) the SO index, which is a standardized index based on the observed Sea Level Pressure (SLP) differences between Tahiti and Darwin (Ropelewski and Jones, 1987); (6) the PDO index, which is often described as a long-lived El Niño-like pattern of Pacific climate variability (Zhang et al., 1997; Mantua et al., 1997); and (7) the NAO index (Barnston and Livezey, 1987), which is based on the surface sea-level pressure difference between the Subtropical High and the Subpolar Low. NAO is a primary mode of atmospheric variability over the Atlantic Ocean and plays an important role in climate variability over eastern North America (Durkee at al., 2007). The monthly timeseries of these seven modes of variability are extracted from NOAA for the period of 1988–2017, and their interannual variability is shown in Fig. 2. Note that for the ENSO index, we considered the Nino3.4 index (Rayner et al., 2003). The annual values for each index are obtained by computing the 12-month average for each index for a given year. While PDO and Nino3.4 have the same interannual variability, one interesting observation is the anti-correlation between PDO and SOI, and between SOI and Nino 3.4. The variability of the AMO shows a negative phase from 1988 to 1995, and a positive phase from 1997 to 2017. Also, the variability of the AO is almost close to that of the NAO with a high positive significant correlation (Lebedeva et al., 2019). PNA varies almost from year to year, with a low amplitude that generally does not exceed +1 in the positive phase, or −1 in the negative phase.

Table 2
Mean annual values and standard deviation of extreme precipitation. The values in bracket are the normalized standard deviation.

Precipitation Indices	Mean Annual values	Standard deviation
SDII	9.88	0.35 (0.017)
PRCPTOT	842.24	66.34 (3.29)
RX1day	61.67	3.34 (0.16)
RX5day	95.96	6.52 (0.32)
R10	26.81	2.11(0.10)
R20	11.45	1.12 (0.05)
RR1	85.07	5 (0.24)
CDD	27.79	2.42 (0.12)
CWD	5.28	0.34 (0.01)

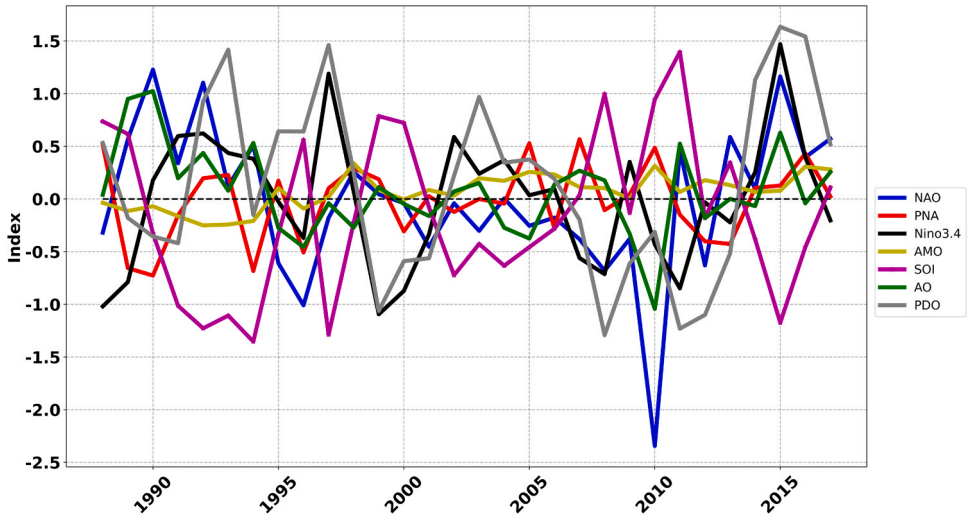

Fig. 2. Interannual variability of the large-scale teleconnections index.

2.2. Methods

2.2.1. Precipitation indices

In this study a set of nine extreme climate indices (Table 1) are computed from daily precipitation datasets to assess the precipitation indices. These precipitation indices have already been used in many climate studies (van den Besselaar et al., 2012; Sheikh et al., 2014; Tian et al., 2016; Li et al., 2017; Frich et al., 2002; Klein Tank et al., 2002). Those indices are amongst the 27 extreme climate indices that have been developed and are highly recommended by the ETCCDI (Peterson et al., 2001; Zhang et al., 2011). The indices under consideration in this study can be divided into three categories: intensity, frequency, and duration (Quan et al., 2020) (Table 1). The intensity indices are the maximum 5-days precipitation amount (Rx5day), the maximum 1-day precipitation (Rx1day), the simple daily intensity index (SDII), and the annual total wet day precipitation amount (PRCPTOT). Note that wet days are days with rainfall amount greater than 1 mm. The frequency indices are the number of heavy precipitation days (R10mm), the number of very heavy precipitation days (R20mm) and the number of wet days (RR1) (R>1 mm). Here, R represents the precipitation event, and the number is the minimum intensity of the corresponding event. The duration indices are the consecutive dry day (CDD) and consecutive wet day (CWD) spells.

2.2.2. Precipitation concentration index

Prior to analyzing the extreme precipitation indices, the temporal distribution of precipitation was checked. To that end, the precipitation concentration index (PCI) (Oliver, 1980) was used. PCI is a powerful indicator of the spatial-temporal rainfall regularity and is important to assessing the seasonal or annual rainfall variability that is an essential feature for water and natural resources management (Zhang et al., 2019). PCI is also a useful indicator of rainfall concentration, floods risk prediction or droughts, and it is calculated on an annual scale according to Eq. (1) (de Luis et al., 2011):

$$PCI_{annual} = \frac{\sum_{i=1}^{12} P_i^2}{\left(\sum_{i=1}^{12} P_i\right)^2} \times 100 \quad (1)$$

where P_i is the monthly precipitation calculated for each rainfall data. According to Oliver (1980), PCI <10 characterize a uniform precipitation distribution (low precipitation concentration); 11<PCI<15 represent a moderate precipitation distribution; 16<PCI<20 denote irregular distribution and PCI> 20 indicate a strong irregularity. Values that range between 16 and 20 represent irregular distribution and PCI >20 characterize a strong irregularity of precipitation distribution.

2.2.3. Mann-Kendall test

One of the techniques of detecting trends in the fields of climatic and hydrological studies is the Man-Kendall trend test (Mann, 1945; Kendall, 1955), which requires data to be independent and randomly distributed. It is a non-parametric test, used to identify monotonic trend and has been widely applied in many climate studies (Zhang et al., 2009; Li et al., 2019; Quan et al., 2020; Shawul and Chakma, 2020; Latif et al., 2021). The null hypothesis in the Mann-Kendall test considers that there are no trends in the time series, whereas the alternative hypotheses states there is a significant trend in the dataset (Shawul and Chakma, 2020). Let $X_1, X_2, X_3 \ldots, X_n$ represent n data points where X represent the data point at time i and n is data length. The statistical formula of the Mann-Kendall test is as follows:

$$S = \sum_{i=1}^{n-1} \sum_{k=i+1}^{n} \mathrm{sgn}(x_k - x_i) \tag{3}$$

where

$$\mathrm{sgn}(x_k - x_i) = \begin{cases} +1 \; if \; x_k - x_i > 0 \\ 0 \; if \; x_k - x_i = 0 \\ -1 \; if \; x_k - x_i < 0 \end{cases} \tag{4}$$

A positive value of S is an indication of an increasing trend, and a negative value of S indicates a decreasing trend. Furthermore, for a sample size that is greater than eight, the statistic S is close to a normal distribution, and the statistic is computed as follows (Zamani et al., 2017; Li et al., 2019):

$$Z = \begin{cases} \dfrac{S-1}{\sqrt{\mathrm{var}(S)}} & if \quad S < 0 \\ 0 & if \quad S = 0 \\ \dfrac{S+1}{\sqrt{\mathrm{var}(S)}} & if \quad S > 0 \end{cases} \tag{5}$$

where $\mathrm{var}(S)$ is the variance of S which can be calculated according to the following equation (Zamani et al., 2017; Li et al., 2019):

$$\mathrm{var}(S) = n(n-1)(2n+5)/18 \tag{6}$$

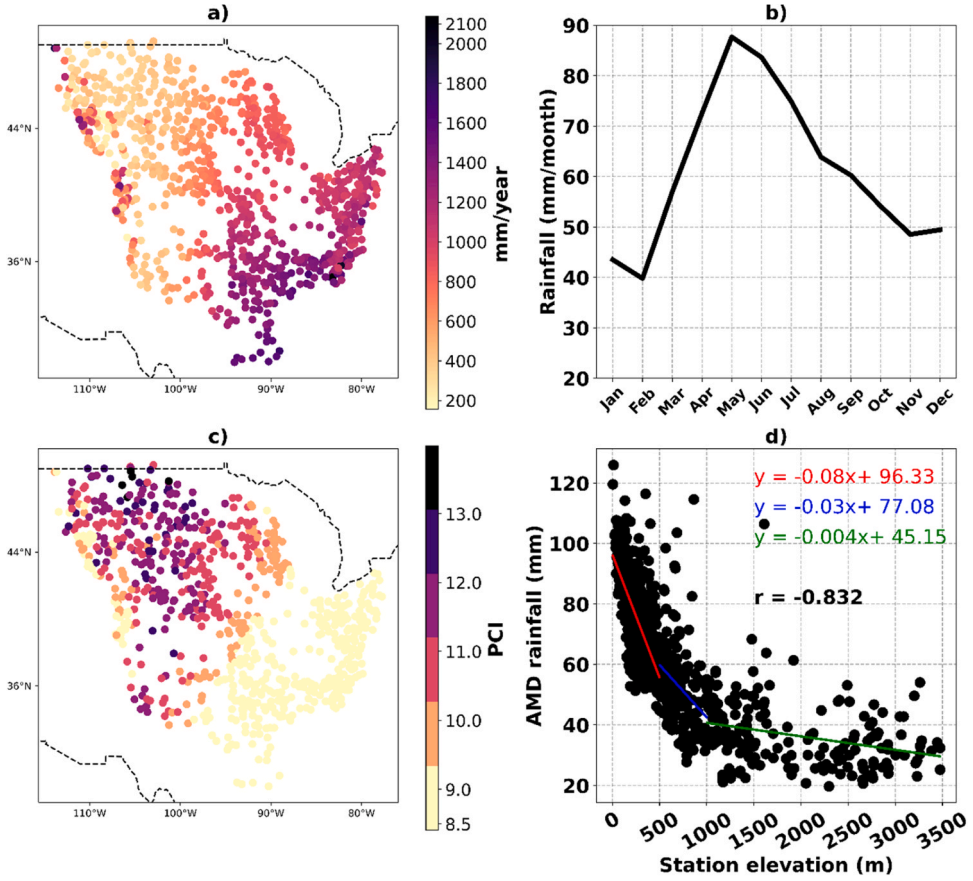

Fig. 3. (a) Spatial distribution of the total annual rainfall (mm/year) and (b) annual cycle of precipitation (mm/month) over the MRB from 729 weather stations for the period 1988–2017. (c) Spatial distribution of precipitation concentration index for the 769 weather stations. (d) Relationship between station's elevation and Annual Maximum Daily (AMD) rainfall for each of the 769 weather stations used in this study. Red, blue, and green lines are linear trends between mean AMD rainfall and elevation range between 0 and 500 m, 500–1000 m and > 1000 m respectively. The linear regression equation for each of the above cited lines is indicated with the same color as the corresponding line. The Spearman's rank correlation coefficient between mean AMD rainfall and station's elevation at two-sided 95 % level is indicated in black bold.

In the bilateral test, if $|Z| \geq Z_{1-(p/2)}$ ($|Z| \leq Z_{(p/2)}$) at the p significant level, the null hypothesis H_o is rejected (accepted). Therefore, under the given confidence level of p, the time series show an upward trend for $Z > 0$ or downward trend for $Z < 0$. Specifically for this study, $|Z| \geq 1.96$ represent the trend of the time series at 95 % confidence level. Given that Mann-Kendall tests results can be influenced by autocorrelation, and that positive autocorrelation might cause the trends test to be rejected, the Hamed and Rao (Hamed and Rao, 1998) method to trends analysis which address serial autocorrelation issues was applied. They suggested the variance correction approach to improve trend analysis. In this approach (see details in Hamed and Rao, 1998) a modified variance is calculated based on the rank of the observations. The rank of the observations is calculated after subtracting a non-parametric trend estimator (Sen, 1968) and only the significant rank are used to calculate the modified variance.

2.2.4. Sen's slope

The magnitude of change and direction (change per unit time) were calculated using Sen's slope approach (Sen,1968). In computational techniques, the Sen slope estimates of N pairs of data are based on the following equation:

$$Q_i = \frac{x_j - x_k}{j - k} \quad for \quad i = 1, \ldots, N, \tag{7}$$

where $x_k and x_j$ are the data values at times j and k (j>k), respectively. If there is only one data in each time period, then $N = \frac{n(n-1)}{2}$ where n is the number of time periods. If there are multiple observations in one or more time periods, $N < \frac{n(n-1)}{2}$, where n is the total number of observations. The values of Q_i are ranked from smallest to largest and the Sen's slope estimator is computed as follow:

$$Q_{med} = \begin{cases} Q_{\left(\frac{N+1}{2}\right)} & \text{if } N \text{ is odd} \\ \dfrac{Q_{\left(\frac{N}{2}\right)} + Q_{\left(\frac{N+1}{2}\right)}}{2} & \text{if } N \text{ is even} \end{cases} \tag{8}$$

Finally, in this study, the two-sided test is employed to test the Q_{med} at 95 % confidence interval and the true slope may be acquired using nonparametric test.

3. Results

3.1. Rainfall characteristics over the Mississippi River basin

3.1.1. Mean spatial pattern and seasonal cycle

The spatial distribution of rainfall exhibits a southeast to northwest gradient, with the largest amount of rainfall recorded over the southeast area of the basin and the lower rainfall amounts recorded over the northwestern part of the domain (Fig. 3a). The southeast and northeast of the MRB, which record the largest amount of rainfall, are known to lack mountain barriers and are exposed to Arctic cold air masses in winter and moist air mass from the Gulf of Mexico in Summer (Almazroui et al., 2021). A few stations with high amount of rainfall are observed at the western borders of Montana. The seasonal variability (Fig. 3b) of rainfall over the MRB is featured by a unimodal cycle with the rainfall peaks of about 100 mm/month in May and the minimum values of about 50 mm recorded in February.

The PCI calculated on the annual scales vary considerably throughout the MRB (Fig. 3c). The annual and seasonal distribution of PCI shows a Southeast to Northwest dipole, with the lowest value of 8.5 located at the Southeastern part of the study area whereas the Northwestern part of the domain exhibits PCI values above 10. The characteristics of the distribution of precipitation over the study domain exhibits both a perfect uniformity of precipitation (PCI<9) (de Luis., 2011) and a moderate precipitation distribution (9<PCI<15) at the annual scale. The spatial distribution of PCI does not match with the spatial distribution of the rainfall (Fig. 3a). In fact, areas with a relatively high amount of rainfall are considered wet areas and are characterized by a perfect PCI distribution whereas areas with low rainfall amount exhibits a moderate precipitation distribution.

3.1.2. Annual maximum daily rainfall

The extreme values in the precipitation data are most of the time related to the occurrences of floods, particularly when they are the main reason for vast water rise (Dušek et al., 2017). The maximum daily rainfall is a parameter that is commonly used to characterize the extreme conditions associated with rainfall intensities and potential flood regions (Shawul and Chakma, 2020). In this study, the AMD rainfall series are analyzed for the 769 weather stations throughout the study area and cover the full range of elevation from lowland/southwestern coastal areas to highland for the period of 1988–2017.

To quantitatively assess the relative dependance between the AMD rainfall and the station's elevation, we calculated the Spearman rank correlation coefficient and performed a two-side t-test at 95 % significance level. The highest mean value of AMD rainfall is 126 mm and is recorded for a station located at sea level. The relationship between the mean AMD rainfall and the elevation behaves in a nonlinear manner (Fig. 3c). However, the mean AMD rainfall decreases as the elevation increases, but the decreasing rate differs for elevation range between 0 and 500 m, 500 m-1000 m, and elevation greater than 1000 m. For instance, for elevation ranges between 0 and 500 m (500 m-1000 m), the decreasing rate of mean AMD rainfall is −8 mm/100 m (-4 mm/100 m). Likewise, for elevation

greater than 1000 m, the decreasing rate of mean AMD rainfall is quite small, −4 mm/100 m. Climate stations located at the altitudes below 500 m mostly exhibit the higher mean values of AMD rainfall (>60 mm) compared to those located at elevations greater than 500 m. The correlation coefficient between the station's elevation and mean AMD rainfall is strong and significant, r= −0.832. The mean AMD rainfall exhibits significant negatives correlation with all the elevation ranges, that is r= −0.56, −0.41 and −0.33 for elevation range between 0 and 500 m, 500 m-1000 m and >1000 m, respectively. This shows that high amount of precipitation may be mostly due to moist air mass from the Gulf of Mexico (Bishop et al., 2018).

3.2. Temporal and spatial analysis of extreme precipitation

The spatiotemporal patterns of precipitation and precipitation-related extremes are considered as the key factors influencing natural ecosystems and human society (Rosenzweig et al., 2002). Thus, the spatial and interannual variability, as well as the trends of the extreme precipitation over the MRB are described in this section.

3.2.1. Temporal evolution

The interannual variability of each of the nine precipitation indices is displayed in Fig. 4 together with slopes that show the linear trends. Each of the precipitation indices is performed for each of the 769 selected weather stations, then, the mean over the study domain is obtained by performing the arithmetical averaging of the precipitation indices obtained from individual long-term stations. The slopes of the significant trends during the period 1988–2017 are displayed in bold. The average value of SDII is 9.88 mm/day with less variability (standard deviation=0.35 mm/day) (Table 2). The SDII (Fig. 4a) shows a very slight (magnitude = 0.01 mm/year)

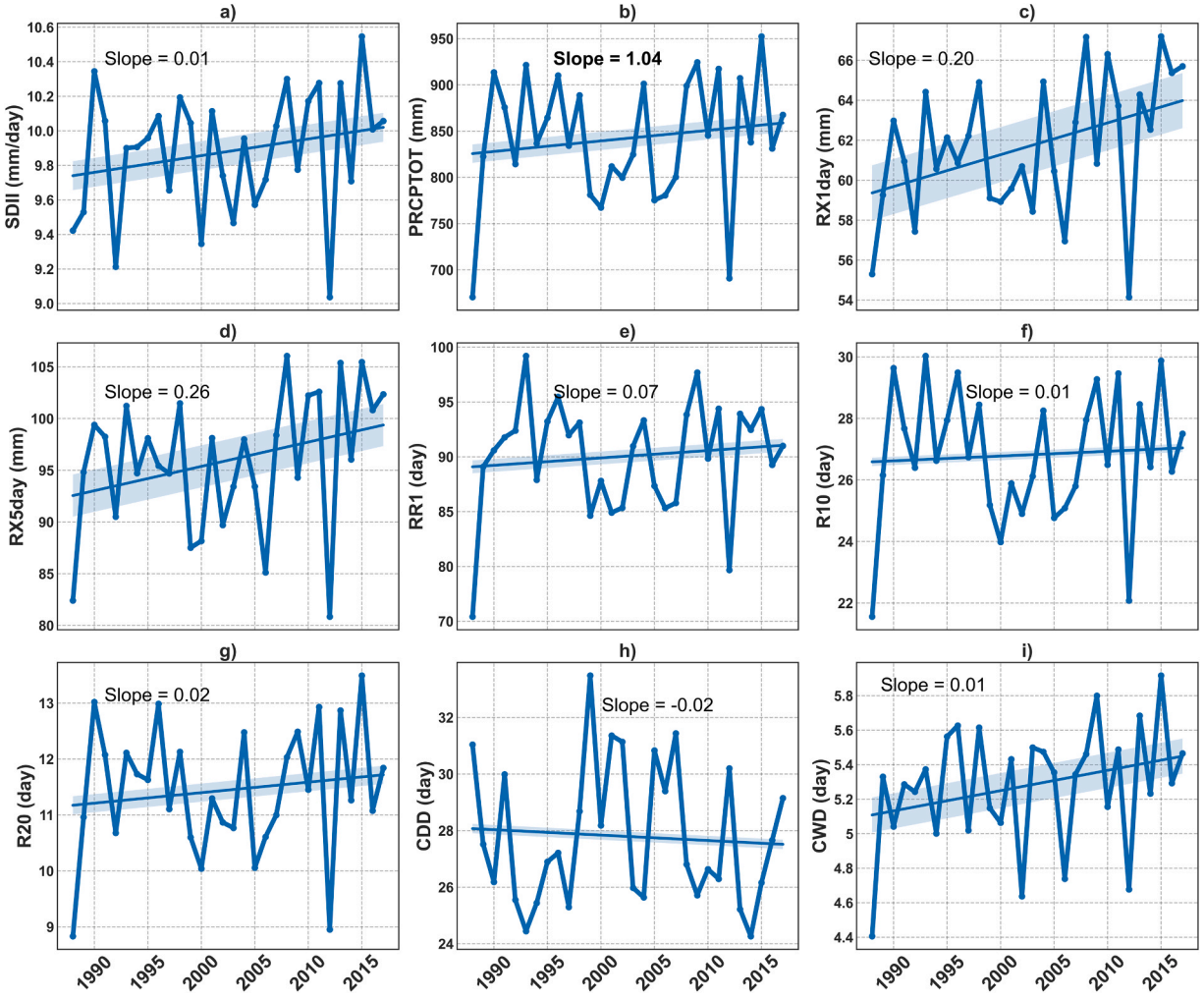

Fig. 4. Temporal variability of the spatially averaged of the nine precipitation indices from the 769 stations for the period 1988–2017: a) SDII, b) PRCPTOT, c) RX1day, d) RX5day, e) RR1, f) R10, g) R20, h) CDD and i) CWD. The solid black lines indicate the trends according to Man-Kendall test at 95 % level. The slopes of the significant trends are indicated in bold.

increasing trend even though not significant according to Man-Kendall test (Mann, 1945; Kendall, 1955). The minimum value of daily precipitation intensity which is about 9 mm/day is observed in 2012, and the maximum which is about ~10.6 mm/day is recorded in 2015. The observed seasonal cycle (Supplemental Information (SI) **Fig. S1b**) of the SDII shows a peak in September, while the wettest month is found to be May with maximum monthly precipitation being about 100 mm (SI, Fig. S1c). The September peak of the SDII is due to abnormally high precipitation intensity observed in September (not shown). In fact, during September, the above average rainfall that fell across the southeastern U.S. are the response to increased southerly moisture transport from Gulf of Mexico, which is almost entirely driven by stronger winds associated with enhanced anticyclonic circulation west of the North Atlantic subtropical high (Bishop et al., 2019). Those winds anomalies enhance water vapor flux over the southeastern U.S., causing an increase in precipitation intensity.

The PRCPTOT (Fig. 5b) shows a significant ($p<0.05$) increasing trend of 1.04 mm/year. This increase in annual rainfall has also been shown by Balling and Goodrich (2010) over the U.S. The maximum value of PRCPTOT over the MRB is about 950 mm/year and is recorded in 2015 during the warm ENSO and the minimum observed value of 670 mm in 1988. As observed with the PRCPTOT, the RX1day (Fig. 4c), and the RX5day (Fig. 4d) show their peak values in 2015, and their minimum is recorded in 2012. The RX1day and the RX5day exhibit an increasing trend; however, they are not significant. The average RX1day (RX5day) is 61.65 mm (95.96 mm), and its standard deviation is about 3.34 mm (6.52 mm). Similar to that of the PRCPTOT, the seasonal variability of RX1day (SI, Fig. S1d) and that of RX5day (SI, Fig. S1e) are unimodal with the maximum values being 32 mm and 50 mm respectively, recorded in May. All the intensity indices (Table 1) show their minimum values in 2012, whereas their maximums are recorded in 2008 (Fig. 4c-d) and the year 2015 (Fig. 4a-b).

The variability of the number of wet days (RR1), the number of heavy (R10mm), and the number of very heavy (R20mm) precipitation days are also analyzed. The RR1 (Fig. 4e) shows an increasing but non-significant trend ($p>0.05$). The minimum and maximum values of 70 days and 94 days are recorded in 1988 and 1993, respectively. The annual mean of the RR1 is 85.07 days (±5 days, one standard deviation). The seasonal cycle of RR1 shows a single peak in May (SI, Fig. S1a) with monthly maximum RR1 being 9.5 days. R10mm (Fig. 4f) and R20mm (Fig. 4g) both show an increasing trend; however, it is not significant. Their mean annual values

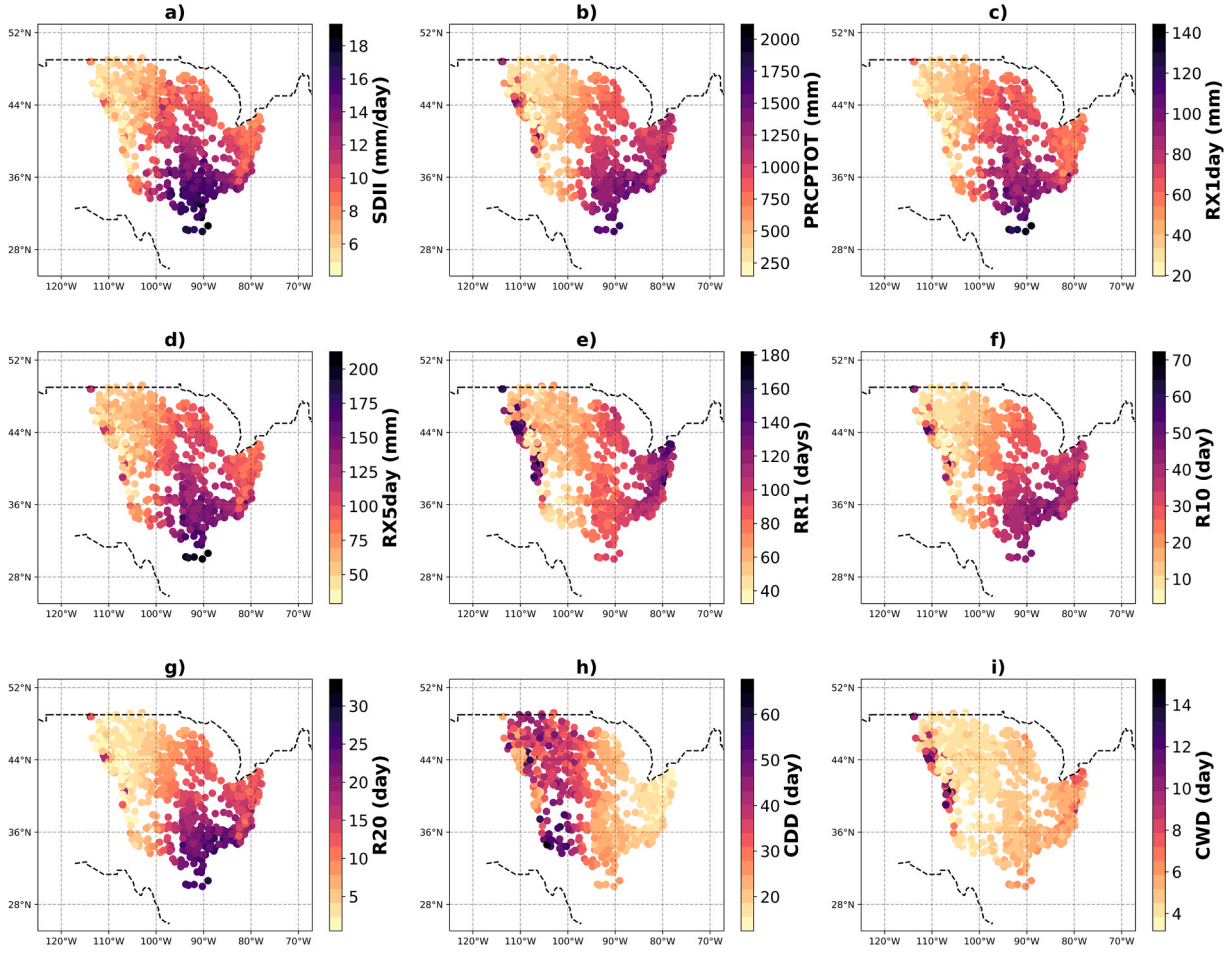

Fig. 5. Spatial pattern of (a) SDII, (b) PRCPTOT, (c) RX1day, (d) RX5day, (e) RR1, (f) R10, (g) R20, (h) CDD, and (i) CWD over the MRB for each of the 769 weather stations for the period 1988–2017. Each of the precipitation indices is defined in Table 1.

are 26.81 days and 11.45 days, respectively, with less variability (Table 2). Their minimum values are observed in 1988 and the maximum values in the year 2015.

Regarding the dry and wet spell, the length of the dry spell decreases slightly whereas the length of the wet spell behaves otherwise, but their trends are not significant (Fig. 5h and i). The annual average length of dry (wet) spell is 27.79 (5.28) days. The seasonal cycle of dry spell shows a double peak. The first peak of about 14 days is observed in January and the second of about 15 days is observed in October (Fig. S1f). For the wet spell, the single maximum of about 3 days is observed in May.

Overall, all the indices exhibit a nonsignificant trend with the exception being PRCPTOT (Fig. 5b). The magnitude of the trend of indices doesn't exceed 0.07 unit per year, except PRCPTOT, RX1day, and RX5day, whose magnitudes are respectively 1.02, 0.20, and 0.26 mm/year. Seven out of nine indices show their maximum values in 2015, recognized as a year that experienced a strong El Niño event (Nigam and Sengupta, 2021), which led to higher precipitation over the southern U.S. The seasonal cycle of the indices exhibits a unimodal cycle with a single peak in May, except for the dry spell and precipitation intensity. The seasonal cycle of the year-to-year

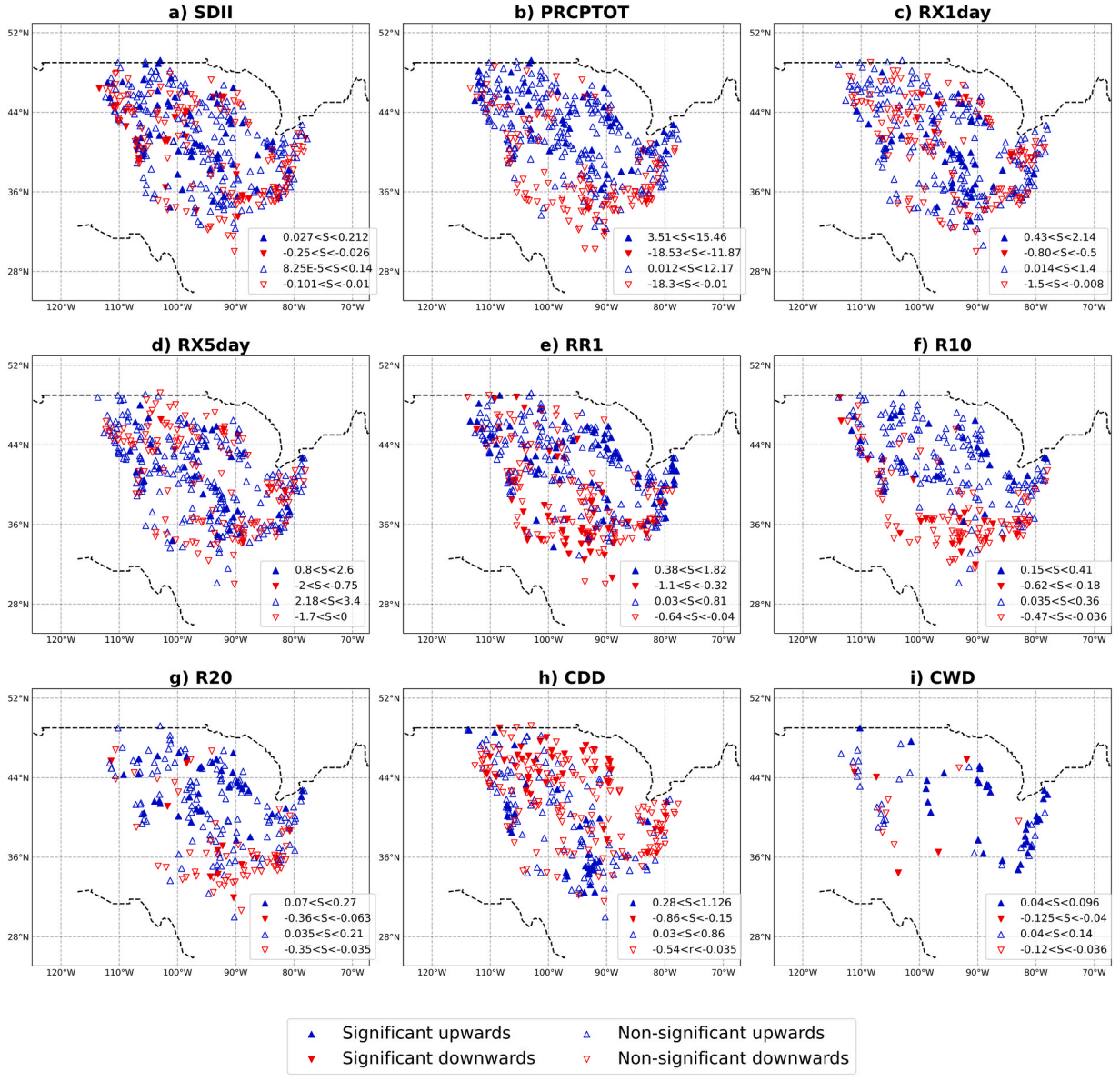

Fig. 6. Spatial distribution of the Mann-Kendall trends of extreme precipitation over MRB for the period 1988–2017; a) SDII, b) PRCPTOT, c) RX1day, d) RX5day, e) RR1, f) R10, g) R20, h) CDD and i) CWD. Upward (downward) triangles denote increasing (decreasing) trends, and solid triangles denote significant trends at 95 % level. The range of the slope on each panel is represented by S. The value of the slope depends on each station and the significance of the slope is not linked to a particular range. Locations with no trend are not shown. Only 50 % of locations with non-significant trends are shown.

(not shown) variability shows abnormally high RR1, PRCPTOT, RX1day, RX5day, R10 mm, and R20 mm in October 2009. Indeed, 2009 is ranked one the wettest years with extreme precipitation in the U.S., particularly over the southeast and eastern U.S. during October in response to hurricane and severe storms activities over the Southeast (NOAA National Centers for Environmental Information, Monthly National Climate Report for Annual 2009, from https://www.ncei.noaa.gov/access/monitoring/monthly-report/national/200913, accessed 02/11/2023).

3.2.2. *Spatial distribution of extreme precipitation and trends*

The spatial distribution of all the precipitation indices (Fig. 5) illustrates a relative same similarity. The highest values are observed in the southern part where precipitation exhibits perfect uniformity (Fig. 3d) and the lowest values are found in the northwestern part of the MRB, except for CDD (Fig. 5h) and CWD (Fig. 5i) which show different spatial patterns. The lowest values of the CDD are observed over the Northeast Ohio river basin whereas the higher values are found in the western MRB (Fig. 5h). The spatial pattern of the CWD (Fig. 5i) exhibits an almost constant value (5 days) throughout the MRB except in the northwestern borders of the domain.

The values of SDII and PRCPTOT range between 5 and 20 mm/day and 250–2000 mm/year, respectively (Fig. 5a-b). The highest values of the SDII (PRCPTOT) are observed in the lower MRB. The northwestern part of the Missouri River Basin and western Arkansas show the lowest values with the indices decreasing from southeast to the northwest. The spatial distributions of the trend analyses for each precipitation indices are presented in Fig. 6. For the SDII, 54 stations show significant increasing trend whereas 26 stations exhibit otherwise (Fig. 6a). For the PRCPTOT (Fig. 6b), 26 stations show a significant increasing trend and only three show a significant decreasing trend which may justify the interannual significant increasing trend of PRCPTOT (Fig. 5b). The decreasing trends of the total precipitation are mostly located over the south of the MRB where SDII also depicts decreasing tendency. The Upper MRB and the Missouri River Basin are experiencing increasing trends whereas the northwestern borders of the Missouri River basin and southeast of Ohio River Basin are experiencing decreasing tendency in PRCPTOT in accordance with the decreasing trend of precipitation intensity.

The RX1day (Fig. 5c) and RX5day (Fig. 5d) have similar patterns to those of the PRCPTOT and SDII. The values of the RX1day (RX5day) range between (20–140 mm) 50–200 mm. For RX1day (RX5day), 32 (24) stations across the MRB show significant positive trend, and 5 (5) stations show significant negative trend (Fig. 6c-d). Most of the stations showing increasing trends are located over the central MRB and to a lesser extent over the northeast where they are mixed with stations experiencing decreasing trend (Fig. 6c & d).

The number of wet days (RR1) (Fig. 5e) ranges from 40 to 180 days. The highest numbers of RR1 are found in northeast Ohio River Basin and for some stations in the western borders of Missouri River Basin. Nevertheless, the distribution depicts a west to east gradient, with the western part experiencing the lower number of wet days. The spatial distribution of the trend of RR1 (Fig. 6e) shows that stations with significant decreasing trend are mostly located over south (i.e., lower Mississippi, Red and southeast Ohio River Basins) whereas those with increasing trend are at the northern MRB and at the northeast Ohio River Basin. R10mm (Fig. 5f) and R20mm (Fig. 5g) show the same spatial distribution but differ in intensity. For instance, their values vary between 10 and 70 days and 4–30 days for R10 mm and R20 mm respectively. In contrast, almost all the stations with significant increasing trends in heavy (Fig. 6f)

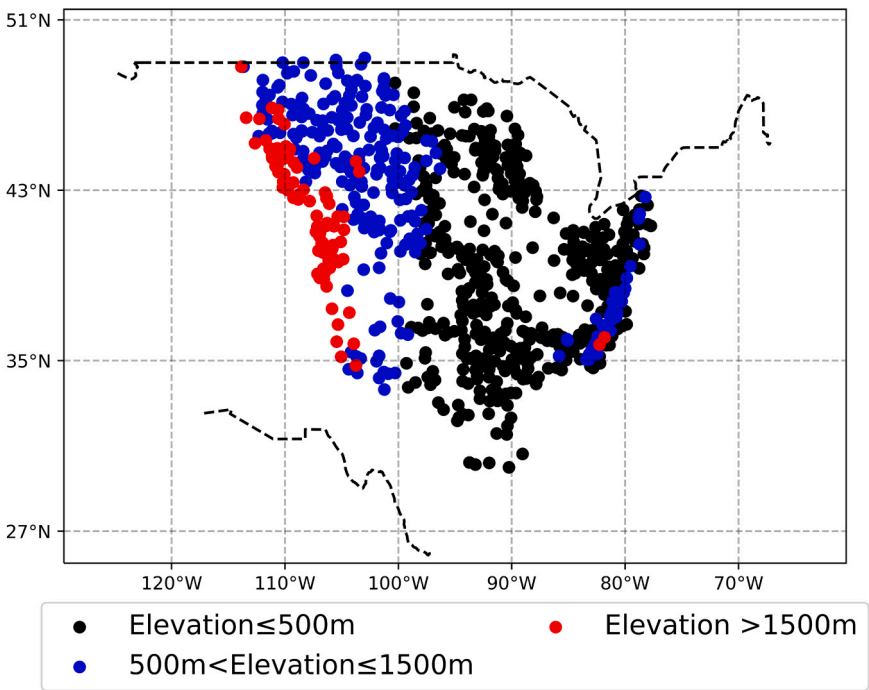

Fig. 7. Station elevations over the MRB. Elevations are separated into three categories. Elevations below 500 m (black dots), elevations range between 500 and 1500 m (blue dots) and elevations above 1500 m (red dots).

and very heavy (Fig. 6g) precipitation are located over the Missouri, Upper Mississippi, and Ohio River Basins. Decreasing trends are mostly over the Arkansas River Basin, Lower MRB and Tennessee Region.

Drier conditions as indicated by dry spell duration ranges from 15 to 65 days and show and east to west gradient (Fig. 5h). Most of the stations with significant decreasing trends are in the northern Missouri River Basin, the Upper MRB, and the northeast Ohio River Basin. Stations with increasing trends are confined to the lower MRB (Fig. 6h).

Unlike dry spells, wet spells (Fig. 5i) show almost a constant spatial pattern across the MRB with duration not exceeding 14 days. In fact, almost all the stations show length of CWD below six days with the exception of a few stations located in the western borders of the domain where the maximum number of cumulative wet days reaches 13 (Fig. 5i). The number of stations recording significant wet spell represents only 5.20 % of the total weather stations considered. That is, 40 stations show a significant trend of wet spells, of which 35 stations show significant positive trend and five stations show significant negative trends (Fig. 6i). Overall, the results reveal interesting details such as: (1) a west to east gradient characterizing the spatial pattern of the intensity and frequency indices (Table 1); (2) an east to west gradient is the main feature of the spatial distribution of the dry spell; (3) the spatial distribution of the wet spell is flat with the duration not exceeding six days except for a few stations in the western borders of the domain i.e., western Montana; (4) the lower Mississippi, Red, and south Ohio River Basins are experiencing decreases in SDII, PRCPTOT and also in number of wet days; (5) the frequency of heavy and very heavy precipitation is decreasing over lower Mississippi, Red, and south Ohio River Basins and is increasing over the Upper Mississippi, Missouri, and north east Ohio River Basins; (6) Louisiana is experiencing an increasing tendency in the duration of dry spells; (7) southeast Ohio River Basin and some stations over the Upper MRB show significant increasing trend in the duration of wet spell; and (8) most part of the domain does show no trend in the duration of wet spells.

3.3. Factors influencing precipitation indices and trends

3.3.1. Elevation dependance

The spatial patterns of the extreme precipitation studied here are also controlled by the pattern of surface elevation. For instance, above 500 m of high (Fig. 7), the intensity indices (Table 1) are weak or diminish considerably, however there is a persistent high amount of PRCPTOT (Fig. 5b) particularly over the western border of the domain. Regarding the frequency indices (Table 1), their values are low above 500 m with the exception being for the number of wet days whose maximum values are shifted to the North Ohio basin and to the western border of Missouri River basin (Fig. 5e) where elevation is greater than 1500 m (Fig. 7). This indicates another process that may come into play and deserves to be discussed in section 6. Regarding the duration indices, dry spells (Fig. 5h) are mostly longer for elevation between 500 m and 1500 m whereas wet spell (Fig. 5i) seems to be longer above 1500 m.

To quantitatively evaluate the interdependence of precipitation indices with the topography, the spearman correlation coefficients are calculated at 95 % level between each precipitation index and elevation (Table 3, Fig. S2). At first glance, the extreme indices are strongly correlated with the elevation, especially elevation below 1500 m (Fig S2, Table 3). Below 1500 m, the indices are significantly negatively (except CDD, r=0.54) correlated with the elevation exhibiting a rapid decreasing in indices as the elevation increases. Similarly, the slope (Sen's Slope) also decreases with the elevation (Fig. S3). Above 1500 m, since the number of wet days is significantly increasing with the elevation (r=0.66, Fig. S2, Table 3), this has a significant impact on PRCPTOT, the R10mm and the length of wet spells (CWD) which also increase with correlation being, 0.54, 0.50, 0.64 respectively (Fig. S2, Table 3). As the length of wet spells is increasing with elevation, it thus decreases the length of dry spells. The impact of increasing number of wet days on very heavy rainfall above 1500 m is noticeable, but not significant. This imply that, the low elevated areas are more susceptible to flooding following the damage of dams and dikes due to extreme rainfall.

Over the entire MRB, there are no significant temporal trends except for PRCPTOT (Fig. 4) as indicated in section 4.1. Because the

Table 3
Spearman correlation coefficient between precipitation index and station elevation.

Precipitation indices	Elevation (m)	Correlation
SDII	≤ 1500	−0.74*
	1500–3500	−0.07
PRCPTOT	≤ 1500	−0.75*
	1500–3500	0.54*
RX1day	≤ 1500	−0.78*
	1500–3500	−0.15
RX5day	≤ 1500	−0.78*
	1500–3500	0.14
R10mm	≤ 1500	−0.72*
	1500–3500	0.50*
R20mm	≤ 1500	−0.79*
	1500–3500	0.18
RR1	≤ 1500	−0.53*
	1500–3500	0.66*
CDD	≤ 1500	0.54*
	1500–3500	−0.50
CWD	≤ 1500	−0.50*
	1500–3500	0.64*

* Indicates significant correlation at 95 % level ($p<0.05$).

spatial pattern of the precipitation indices is controlled by the elevation, the temporal trends of the extreme are analyses in three subdomains (Fig. 7) to evaluate the influence of topography. However, we couldn't find any significant trends over the subdomains, except for RX1day and CWD over the area with elevation below 500 m (not shown).

3.3.2. Moisture flux

To further investigate the potential divers of extreme precipitation, the mean vertically integrated horizontal moisture flux from the surface to 850 hPa expressed as:

$$Total\ mositure\ flux = \quad g^{-1} \int_{surface}^{850hPa} qv\ dp \tag{9}$$

is calculated using monthly ERA5 dataset from 1988 to 2017. Here g is the gravitational acceleration ($m.s^{-2}$), v is the horizontal wind vector ($m.s^{-1}$), q is the specific humidity ($g.kg^{-1}$) and p is pressure (hPa). The result is shown in Fig. 8. There is a good agreement between the pattern of moisture flux and that of the annual total wet day (Fig. 5b). The south to northeastern part -encompassing Lower Mississippi, Tennessee and Ohio region- is fed by the southeasterly to westerly tropical winds over the southern part of the MRB which increases the local moisture with impact on precipitation. Prior work has shown that over the U.S., most of the increasing trends in total annual precipitation mostly come from the Eastern U.S. due to the increasing trends of southerly winds which transport moisture from the Gulf of Mexico toward the southeastern and Eastern part of the MRB (Bishop et al., 2019). Since the PRCPTOT is highly correlated (Fig. S4) with other indices (except CDD), we therefore conclude that any change in PRCPTOT is likely to reflect on extreme precipitation.

3.3.3. Dependance to temperature

It has been shown that temperature is increasing in the U.S. since the last four decades and the consequences on precipitation vary from season to season (Shenoy et al., 2022). With the aim to understand the spatial distribution of the trend of extremes precipitation (Fig. 6), the spatial distribution of the mean, maximum and minimum temperature trends from Climatic Research Unit (CRU) for the period 1988–2016 is shown in Fig. 9. The modified Man Kendall trends test (Hamed and Rao, 1998) is applied on each pixel to evaluate the trend. Fig. 9 shows that almost all part of the MRB (except North Missouri region with is experiencing decreasing in temperature components) is experiencing an increasing in mean temperature (Fig. 9a) and minimum temperature (Fig. 9b), with most of the significant trends located over the southern part of the domain encompassing, Lower Mississippi, Tennessee, Arkansas and south of Missouri region. The Arkansas region and Lower Mississippi are experiencing a rapid increase in maximum temperature.

Decreasing trends in extreme precipitation indices such as PRCPTOT, RR1, R10mm, and R20mm are found mostly where the temperature components are significantly increasing. In the same vein, over the northern part where temperature components show decreasing trends-even though not significant- previous cited indices are showing evidence of significant increasing trends. However, the length of dry and wet spells is likely to be more tied to the trend of maximum temperature. Over, the Northeast Ohio river basin, which is experiencing non-significant decreasing in maximum temperature, there is an increasing (decreasing) tendency of the length of wet (dry) spells. Overall, the increasing in temperature is likely to increase the dry spells and vice versa. Though, the spatial pattern of the trends of extreme precipitation indices cannot be totally explained by the pattern of temperature, pointing to other factors that may play a significant role.

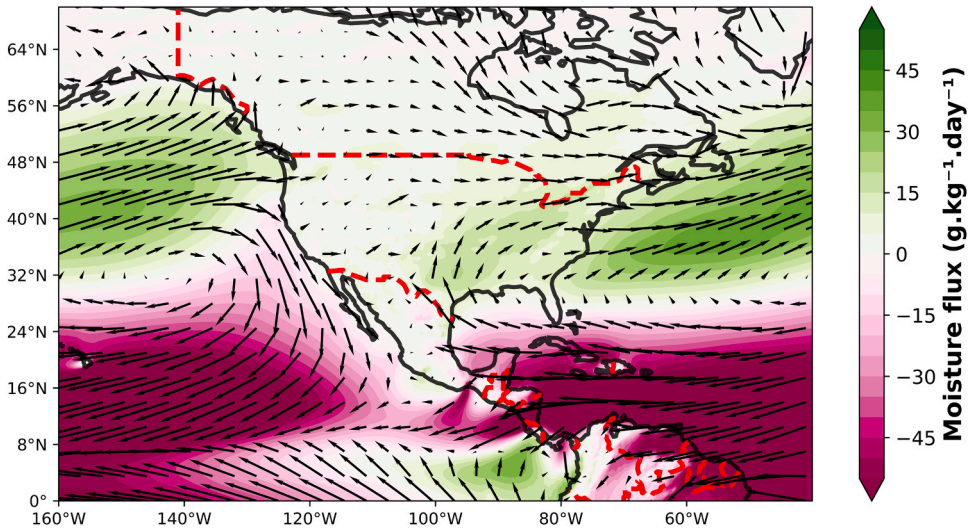

Fig. 8. The vertically integrated averaged moisture flux from ERA5 data for the period 1988–2017.

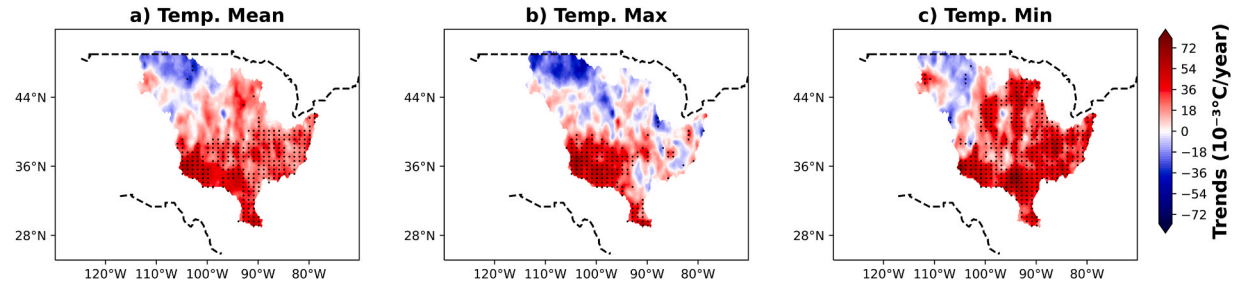

Fig. 9. Spatial trend of the temperature components from CRU data for the period 1988–2016. (a) mean temperature, (b) maximum temperature and (c) minimum temperature. The magnitude of the trend is calculated using Sen slope approach described in Section 2.2.4. The black dots indicate areas with significant trends at 95 % level.

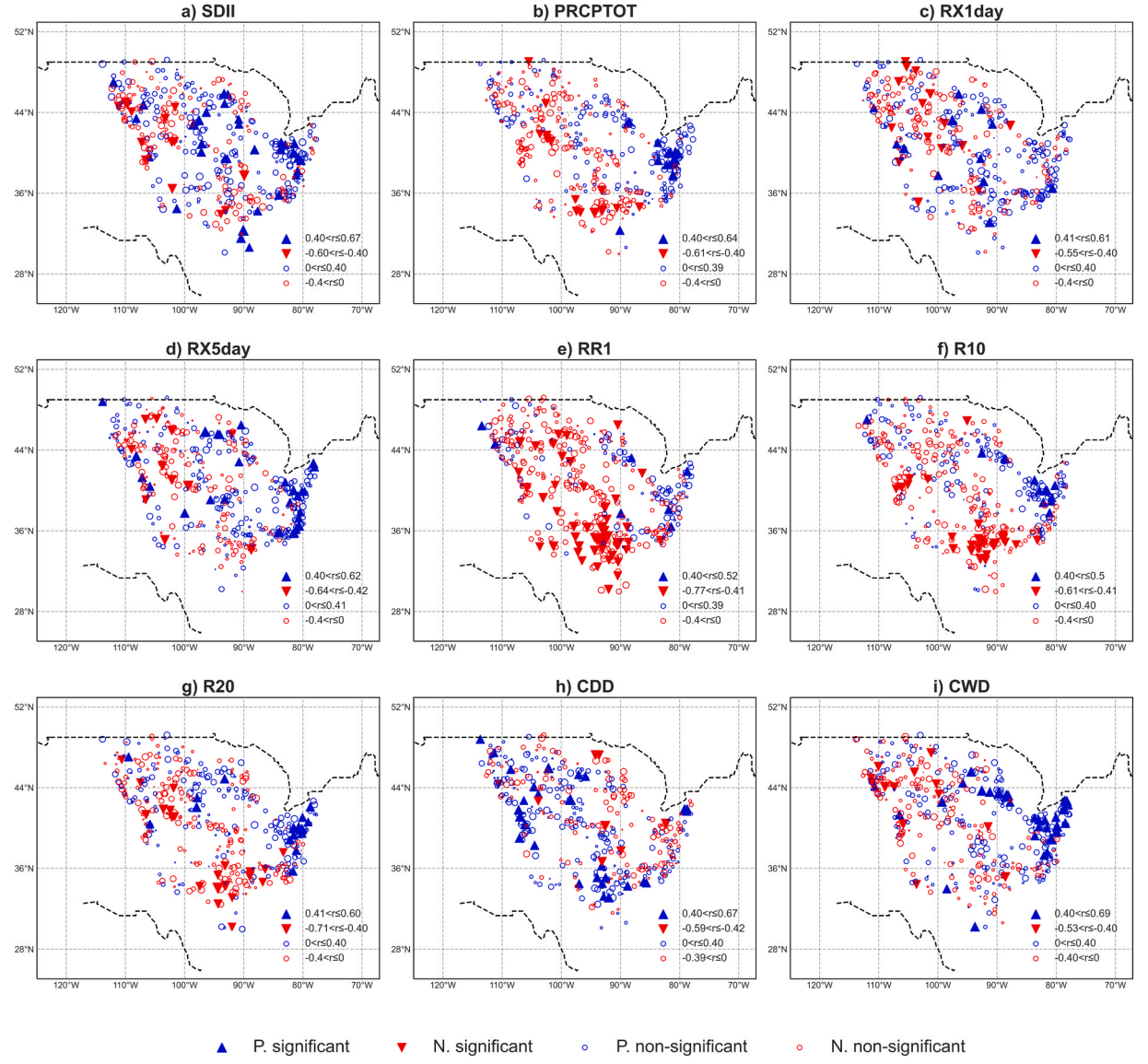

Fig. 10. Spearman partial correlation between precipitation indices and AMO for the period 1988–2017. Blue (red) up (down) triangles indicate positive (negative) significant correlations. Blue (red) circles indicate positive (negative) non-significant correlations. Results are valid on annual scale at 95 % level of significance. Only 50 % of non-significant correlation are shown.

3.3.4. Large-scale patterns of atmospheric and oceanic circulation

To determine if the temporal evolution or spatial pattern of the trends of extreme precipitation (Table 1) over the MRB are related to any sources of interannual or interdecadal variability, the associated relationship between large scale modes of variability and precipitation indices over the study area is investigated through the partial correlation analysis between the regional average of the precipitation indices and seven modes of variability described in **Section 2.1.2** for the period 1988–2017. The partial correlation (see details in Wang, 2013) is applied on each teleconnection index to take away the influence of the remaining six teleconnections. The results presented in Fig. S7 show the average values of the partial correlation between yearly timeseries of the stations that exhibit positive and negative correlations as well as the significance of the correlations.

Overall, none of the large-scale modes of variability on average shows a strong correlation with extreme precipitations over the whole MRB. The average values of the correlation for stations that exhibit significant (non-significant) relationships between extreme precipitation and each mode of variability vary between −0.5 and 0.5 (-0.2 and 0.2) (Fig. S7). To assess the net effect of each mode of low frequency variability over the domain, we calculated the mean value of each of the precipitation indices by averaging the 769 stations to obtain a single time series, then we ran the Spearman partial correlation between precipitation indices and each mode of variability at 95 % level. It is worth mentioning that the correlations are weak. Also, none of the correlations' coefficients between the indices and large-scale teleconnections is significant (Fig. S7, red line) for the entire domain. However, the strength of the links between teleconnections and precipitation indices varies from to point-to-point location. For instance, AMO is generally non significantly

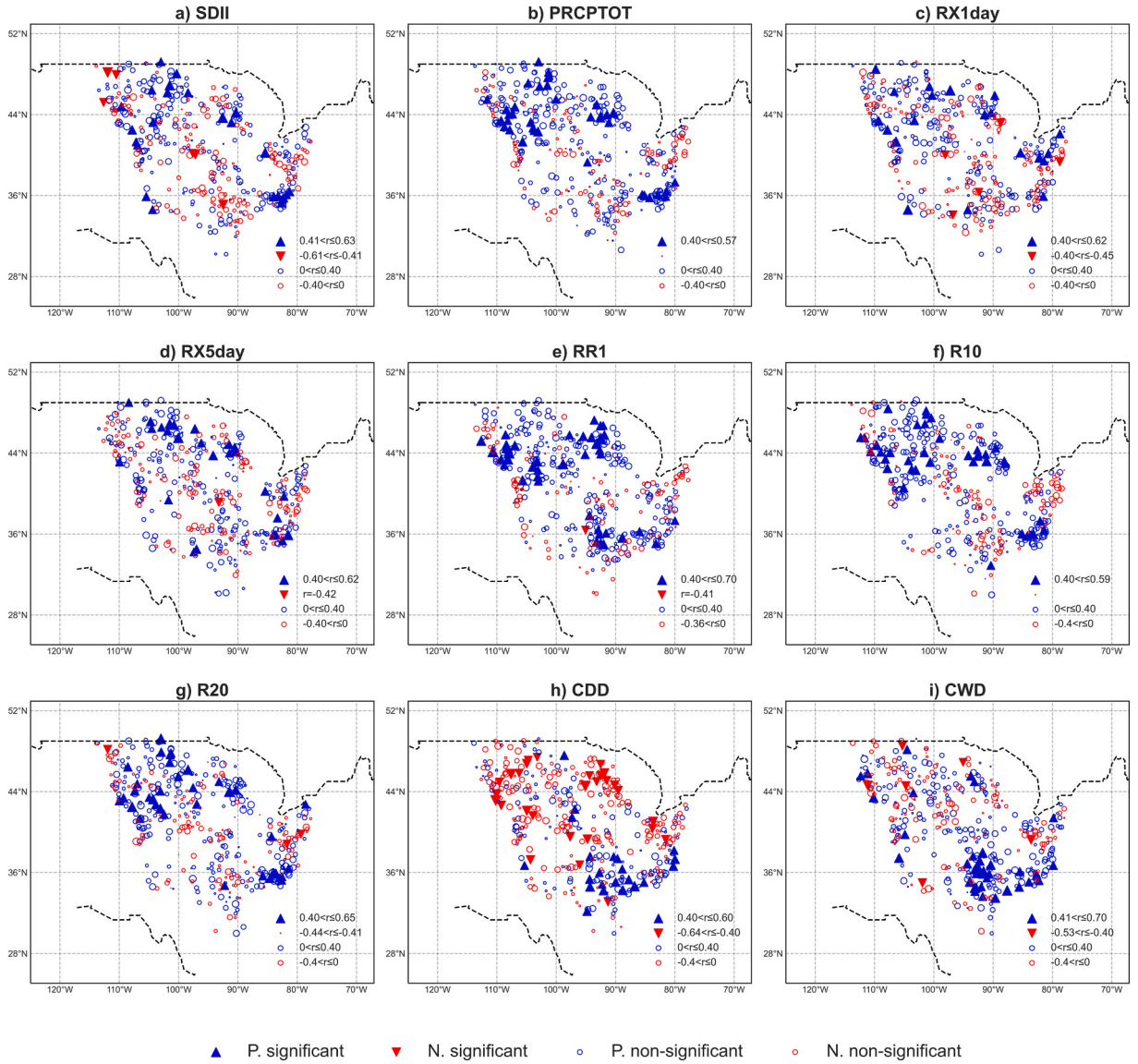

Fig. 11. As Fig. 10 but between precipitation indices and North Atlantic Oscillation.

correlated with intensity indices over most part of the domain (Fig. 10a-c). However, significant positive correlations are typically over the Upper Mississippi and Northeast Ohio river basin whereas the western and southern part is mostly negatively correlated with AMO particularly the PRCPTOT (Fig. 10b). The negative relationship between SDII and AMO is shown for stations located in the Red River basin, and northwestern border of Missouri river basin. Consistent with Enfield et al., (2001), a positive relationship with SDII is noted for southern Louisiana and southeastern and Upper Mississippi. This positive relationship is likely due to an increase in hurricane activity that affected Florida and the coastal southeastern U.S. (Curtis, 2007) as the AMO warm phase begin again in 1995 with a general increase of precipitation in the U.S. (Balling and Goodrich, 2010). For RX1day (RX5day) (Fig. 10c-d), a positive relationship with AMO is observed in the south and north Ohio river basin, the north Upper MRB, and at the northwestern borders of Montana. Negative relationships are mostly found in North Dakota, Montana, and in the northern part of Louisiana (Fig. 10c-d). The relationship with frequency indices (Table 1) shows negative significant correlations at the southern part of the domain encompassing Ohio, Arkansas, Red, southern Missouri, and the lower MRB with an exception being for some stations located at Oklahoma state which show otherwise. Positive relationships between frequency indices (Table 1) and AMO are mostly shown by stations at the northern part of the Upper Mississippi and northeastern part of the domain (Fig. 10e-g). As AMO decreases the frequency of heavy and very heavy precipitation over the lower MRB and western part of the domain, it conversely increases the length of dry spells over the above-mentioned locations (Fig. 10h). Several studies (Sutton and Hodson, 2005; Enfield et al., 2001) have reported that drought over North America is related to the AMO warm phase in response to reduced rainfall due to low pressure anomalies. For wet spells

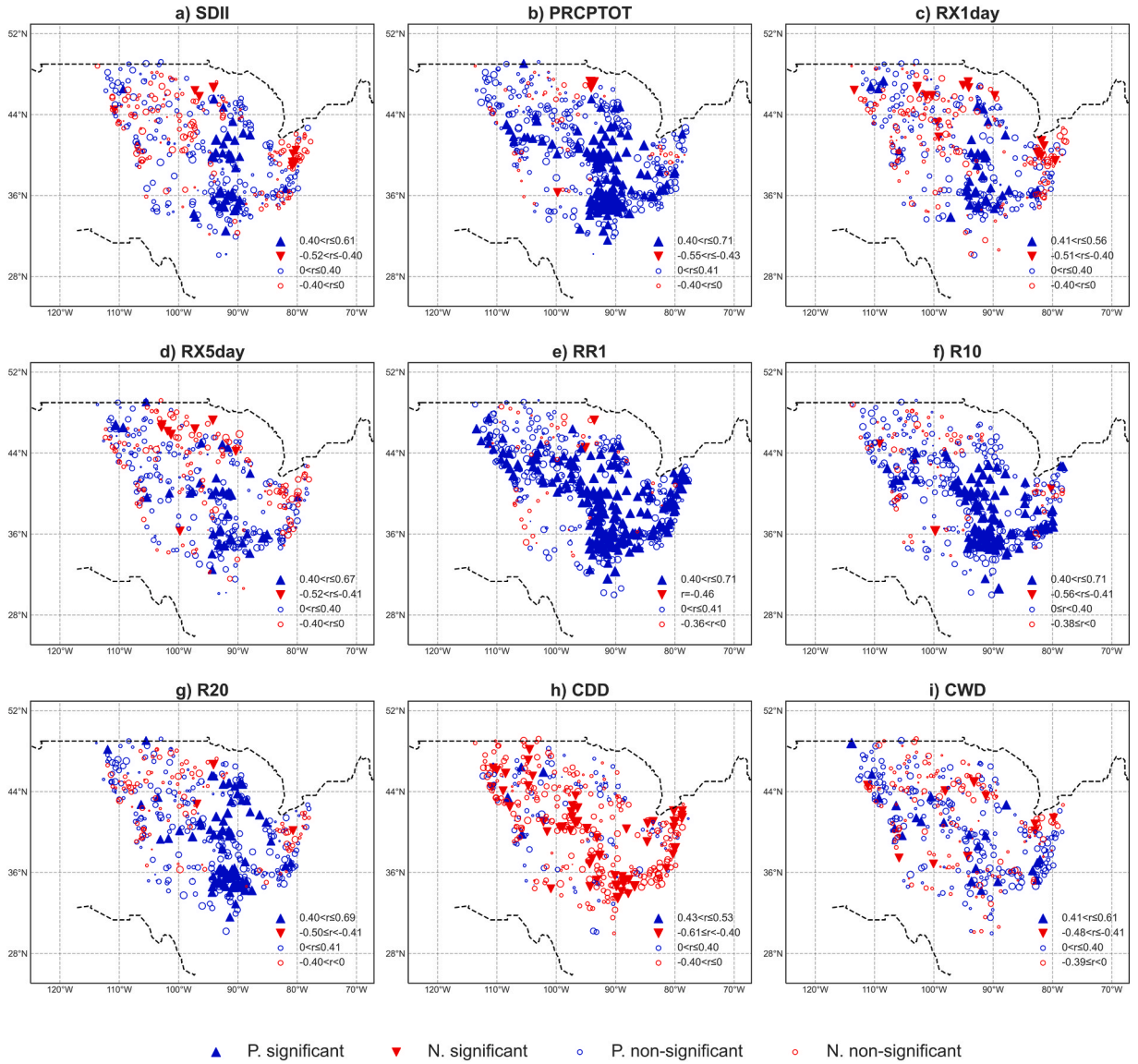

Fig. 12. As Fig. 10 but between extreme precipitation and El Nino Southern Oscillation.

(Fig. 10i), stations located in the northeast Ohio River Basin and over most of the Upper MRB have a positive relationship with AMO consistent with the increasing trends of CDD (Fig. 6). Usually, AMO shows positive relationship in the locations where precipitation indices show increasing trends and negative relationship otherwise. Overall, AMO contributes significantly to reducing the rainfall amount over the MRB by increasing the length of dry spells.

The NAO is the primary mode of atmospheric variability over the Atlantic Ocean and plays an important role in climate variability (van Loon and Rogers, 1978; Greatbatch, 2000). This holds true over the MRB (Fig. 11) where NAO has positive significant correlations with intensity (Fig. 11a-d) and frequency (Fig. 11e-g) indices, particularly over the northern part of the MRB and Tennessee region. This align with Durkee et al., (2007) who showed that the statistically significant increases in the frequency of the observed precipitation across the eastern U.S. is associated with the positive phase of the NAO. In fact, this positive correlation with the NAO may be due to the increases in moisture flux along the east coast of the U.S. (Hurrell, 1995) or/and the increase of the warm air and moisture advection into the eastern U.S (Hurrell and Dickson, 2005) caused by an increased pressure gradient among the subtropical North Atlantic regions. Interestingly, NAO may produce warmer (Fig. 11h), wetter (Fig. 11i) conditions over the southern part of the MRB. With an exception being for dry spell (Fig. 11h), which exhibit a negative relationship over the third quarter of the entire domain, NAO's positive influence on precipitation indices (Table 1) is most pronounced over the southeast, the Upper MRB and northwestern part of the domain. Over the northeast Ohio River basin, stations exhibit non-significant negative correlation with frequency indices, while few are positively correlated with intensity indices.

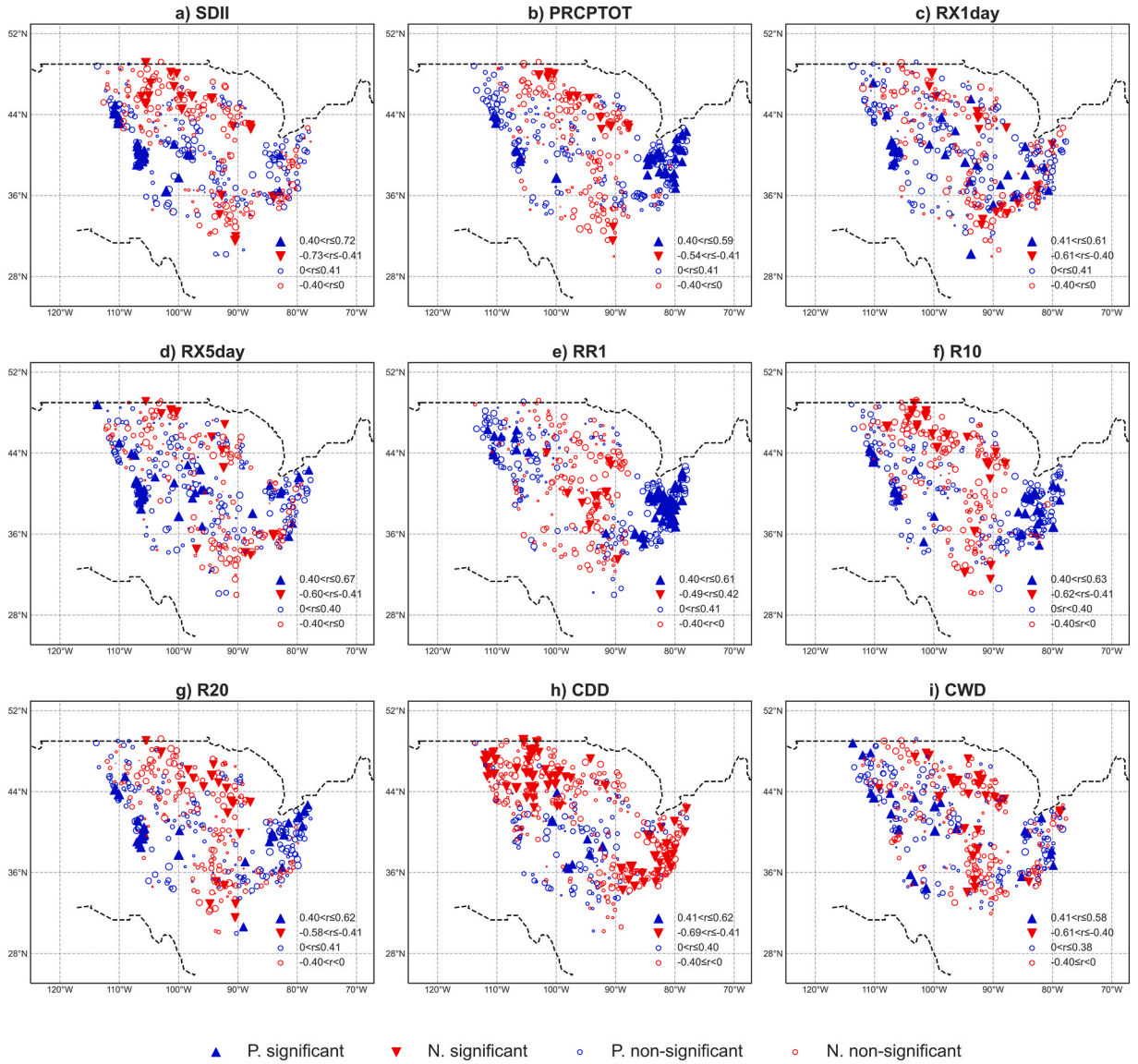

Fig. 13. As Fig. 10 but between precipitation indices and Pacific Decadal Oscillation (PDO).

The relationship between ENSO and extreme precipitation indices (Fig. 12) shows positive correlations almost all part of the MRB, except with the CDD which exhibits negative correlations over the entire domain. For the frequency indices (Fig. 12a, c &d) negative correlations (few are significant) are observed over the central and northern Missouri basin encompassing Wyoming, Montana, North and South Dakota. The most significant positive correlations are observed over the southern and Upper Mississippi. This is particularly true for PRCPTOT (Fig. 12b) which exhibit strongest positive correlation (r=0.71) with ENSO, indicating that ENSO is one of the most important climate indexes generating precipitation over the MRB: (1) by increasing the number of wet days event (Fig. 12e), (2) responsible of heavy (Fig. 12f) and very heavy (Fig. 12g) precipitation, (3) increase the amount of annual precipitation (Fig. 12b). The occurrence of ENSO will dismiss longer dryness (Fig. 12h) by prevailing wetting conditions over the MRB. However, the length of wet spells seems to be not strongly tied to ENSO even though they are positively (few are significant) correlated over most part of the domain. It is interesting to note that, although ENSO and SOI Oscillate oppositely (Fig. 2), they almost have the same spatial relationship with the extreme precipitation indices and that the observation made for ENSO are valid for SOI (Fig. S8).

The relationship between PDO and precipitation indices is shown in Fig. 13. The pattern of the correlation between PDO and extreme precipitation indices are quite similar, except the CDD. The northern, and southern through the central part of the MRB are featured by significant negative correlations, even though not too strong. Conversely, the northeastern -encompassing Tennessee Region and Ohio River basin- and western border of the domain exhibit strong significant positive correlations with PDO. This will enhance the SDII and PRCPTOT over the western borders and Ohio river basin. However, with the decreasing of number of wet days,

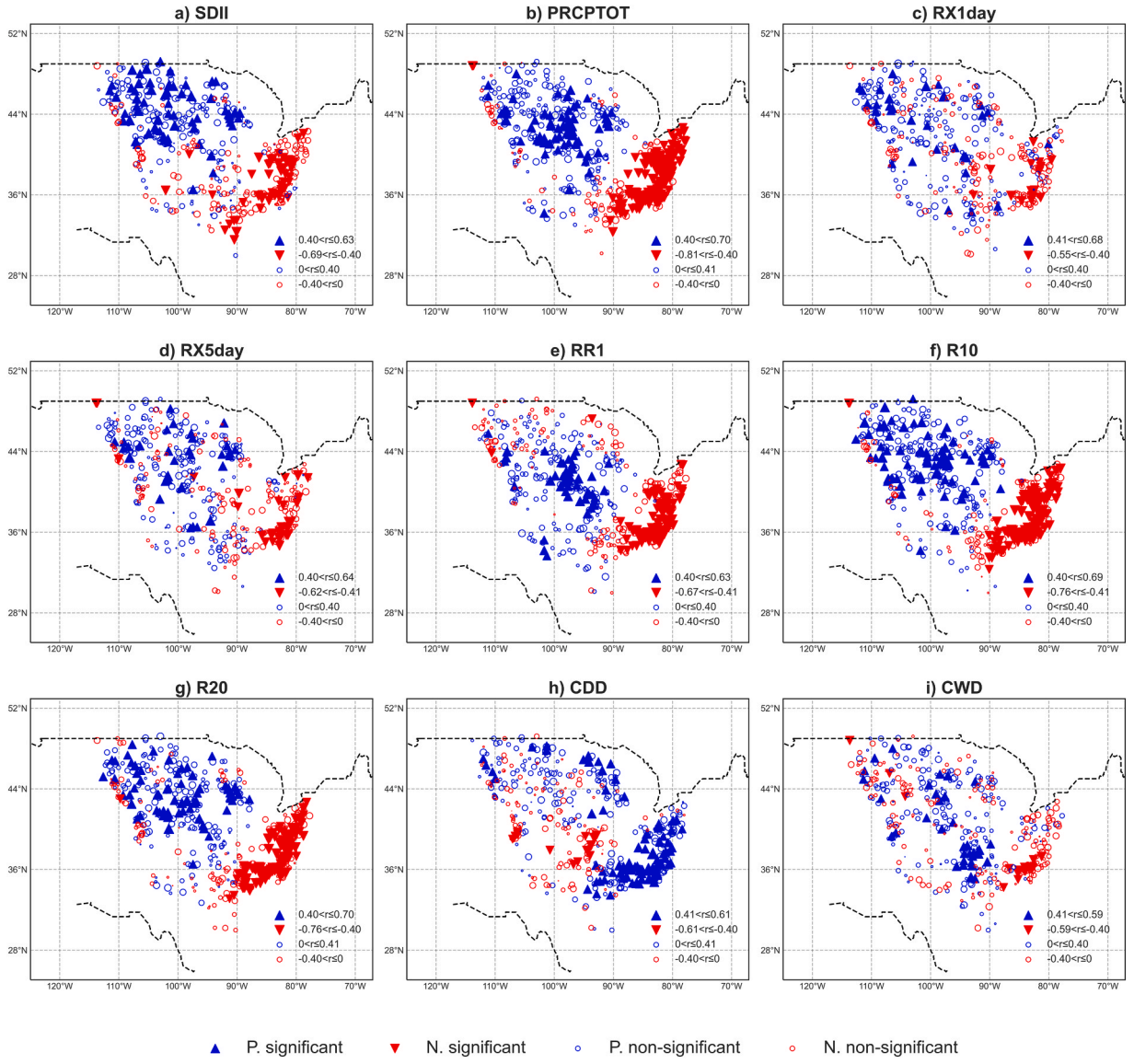

Fig. 14. As Fig. 10 but between precipitation indices and Pacific North America.

Oklahoma, Kansas, and Missouri states are experiencing persistent dry spell events (Fig. 13h) due to PDO. Regarding the RX1day (Fig. 13c) and RX5day (Fig. 13d), negative correlations are shown with stations over the Southeast and North Dakota.

The relationship between PNA and extreme precipitation (Fig. 14) shows a clear distinction between areas with positive relationships and those with negative relationships. Our results indicate that there is a strong connection between PNA and precipitation indices (Fig. 14a-g & i) (except CDD) over the entire northern part of the domain encompassing the entire Missouri river basin, Upper Mississippi, and the Arkansas River Basin where stations display statistically significant positive relationships. For CDD (Fig. 14h), the positive relationships are found for stations located at the southern part of the domain, over the Ohio River basin and over the Upper Mississippi where correlations are significant and strong. Arkansas, Oklahoma, Missouri, and Kansas states are experiencing negative relationship between CDD and PNA (Fig. 14h). The significant negative relationships are mostly found at the southern and the northeast parts of the Ohio River Basin for frequency and duration indices (Table 1) as well as for the duration of the wet spell. Mallakpour and Villarini (2016) have also found negative relationships between PNA and the frequency of heavy rainfall (Fig. 14f) over the southern and southeastern parts of the U.S. Non-significant negative correlations can be found for some stations at the northern part of the MRB especially in Montana and North Dakota for RR1 (Fig. 14e).

The relationship between AO and the extreme precipitation indices studied here are shown in Fig. 15. Most of the negative correlations with the intensity and frequency indices are observed over the Northern part of the domain and southeast namely the Tennessee region. These negative correlations which are significant and strongest are mostly observed for the PRCPTOT, the RR1 and the heavy precipitation. Positive correlations are observed over the North Ohio River basin, Arkansas and Missouri states. However, negative correlations seem to dominate over northeast of MRB for RX1day. For the duration indices, CDD exhibits significant positive correlations over the northern part of the domain, and negative correlations over the entire south. The CWD is negatively correlated with AO over almost the entire MRB except the northeast Ohio River basin where positive correlations are linked to the number of wet days. Overall, NAO may reduce the precipitation amount over the northern part of the domain while enhancing the length of dry spells. In the other hand increasing rainfall amount -due to NAO-with the occurrence of heavy and very heavy rainfall could be observed over the North Ohio and Arkansas.

4. Discussion

Any change in climatic conditions could cause risks to socioeconomic development or even disaster; thus, the spatiotemporal analysis of the extreme precipitation indices should be studied carefully to guide policymakers and planners. For the analysis of the average extreme precipitation indices, we considered the majors characteristics of rainfall extreme namely, intensity, duration, and frequency. All the precipitation indices are featured by a southeast to Northwest gradient with maximum values over the southeastern part. Generally, the intensity (SDII, PRCPTOT, RX1day, RX5day) indices and frequency of heavy precipitation show the maximum over the Lower Mississippi. This agrees with Bishop et al., (2018) who showed high amount of rainfall over the Southeast Gulf due to increase of southward moisture transport from the Gulf of Mexico (Fig. 8). This increasing in moisture due to southerly wind over the Lower Mississippi can explained more than 94 % of increasing annual total rainfall over the U.S. (Bishop et al., 2018). The strengthening of the southerly wind over the lower Mississippi has a significant impact on the intensity indices. Except the R20mm, the highest values of the frequency indices are observed over North Ohio and western border of the domain where elevations are the highest. It is noteworthy to highlight the control pattern of the extreme precipitation by topography. Almost all the extreme precipitation indices decrease as the elevation increases up to 1500 m except the CDD. Above 1500 m, extreme precipitation indices such as PRCPTOT, RR1, R10 and CWD significantly increase with the elevation. These features of the extreme's precipitation pattern over the MRB haven't been highlighted before. However, we think that mesoscale processes-based assignment such as local convection need to be investigated to better understand the high values of the frequency of wet days and the duration of wet spells over the high elevated area of the western borders.

The spatial patterns of the extreme precipitation trends over the MRB show decreasing trends over the southern part where there is a significant warming and increasing trends over the northern part of the domain for the PRCPTOT and the frequency indices where there is a decreasing in temperature components. Conversely, the dry spell is decreasing over the northern parts and increasing over south. For the intensity indices (except PRCPTOT), there is a mixed of decreasing and increasing to the point-to-point location. However it is hard to compare these trends behavior to the existing literature because of: (1) the lack of studies that analyzed the same extreme precipitation indices over the MRB, (2) studied seasons considered for investigation in previous works versus studied season considered in this study (spring vs annual; fall vs annual; seasonal vs annual) and (3) the chosen threshold to define the extreme precipitation such as top 1 % of days with precipitation, annual daily maximum (Howarth et al., 2019) vs indices evaluated in this work. Nonetheless, for similar studies whose domains cover parts the MRB, some similarities with this work are worth noting. Over the Northeastern U.S. covering part of the Ohio river basin, Griffiths and Bradley, (2007) showed an increasing in R10mm, RX5day and SDII with decreasing in extreme temperature. In the same vein, Balling and Goodrich (2011) demonstrated that the increasing in precipitation intensity over the northeastern quarter of the U.S. is related to the AMO, which is consistent to our findings. Prior work (Villarini and Mallakpour, 2016) showed an increase in the frequency of heavy precipitation over most parts of the U.S. They also mentioned that the control of the heavy precipitation frequency to the variability of Atlantic and Pacific oceans. Our findings also meet these assumptions, as shown by the relationships between extreme precipitation indices and large-scale teleconnections. Similarly, a trend toward warmer and wet conditions (Brown et al., 2010) as well as the increases in total precipitation (Huang et al., 2017) has been found. These finding are also consistent with the present study as the wet spells is increasing over Ohio River basin along with the increasing temperature. In average, the analysis of extreme precipitation indices exhibits an increasing trend (except consecutive dry days, CDD). However, a long-term dataset could be useful to effectively assess the significance and magnitude of the trends of extreme

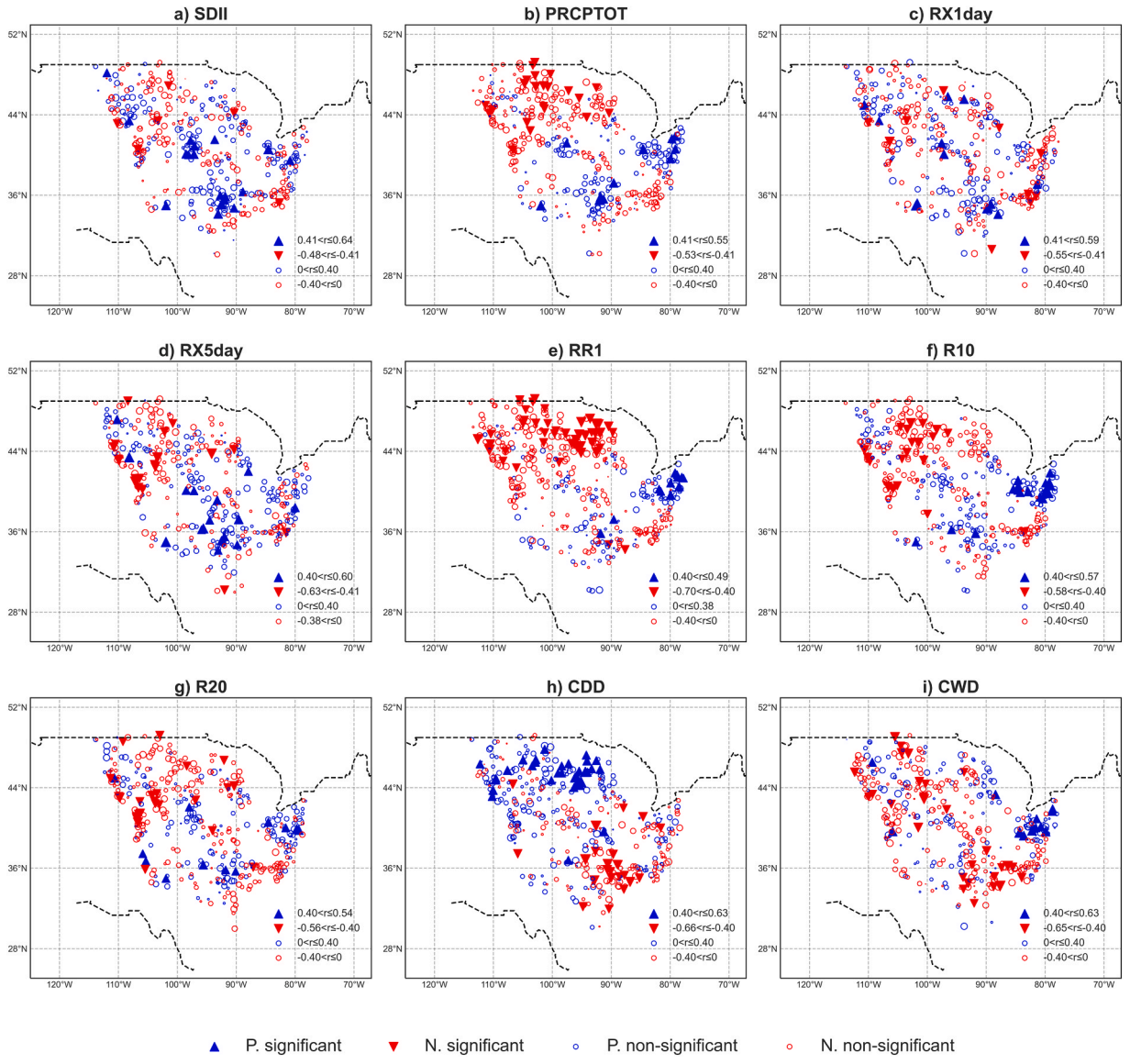

Fig. 15. As Fig. 10 but between precipitation indices and Artic Oscillation.

precipitation indices.

The PRCPTOT exhibits an increase with the magnitude of 1.07 mm/year, indicating that PRCPTOT is the most important index reflecting rainfall variation over the MRB. The increasing trends of frequency indices over the Northern part of the domain could be a good proxy for flooding occurrence. For instance, excessive precipitation produced severe flooding in nine states over the Upper MRB during spring and summer 1993 (Wahl et al., 1993) with the wettest conditions recorded from May through July 1993. It is therefore important that decision makers pay much more attention to the regions where extremes are on the rise. The changes of the mean and variance of the data series primarily show nonstationary (Khaliq et al., 2006). Therefore, the change in frequency and intensity indices, particularly the significant trends of PRCPTOT could be due to a small change in the mean (Mearns et al.,1984). Likewise, an increasing variance could possibly lead to increasing trends of extreme precipitation indices when the climate is in an invariable mean state (Katz and Brown, 1992).

Although taken on average over the MRB, extreme precipitations do not have strong relationships with large scale teleconnections, they do however exhibit strong impact in point-to-point location. There is clear evidence of contrasting effect of large-scale teleconnections on extreme precipitation indices. For instance, while PNA is having negative relationship with the extreme precipitation indices and particularly on heavy and very heavy precipitation over the southeast and positive over the northwest and central MRB, PDO is featuring positive relationship over the northeast and negative from the south to the north through the central domain. Their effects are then likely to counteract. On the same vein, ENSO and/or SOI seem to bring more precipitation over the MRB while AMO is

acting positively only over the northeast Ohio basin. As in this study, positive correlation between SOI, NAO and heavy rainfall over Ohio and Indiana has also been found by Mallakpour and Villarini, (2017) at the annual scale. Similarly, there is certain agreement between this work and Mallakpour and Villarini, (2017) findings' regarding the relationship between AMO and heavy rainfall. However, there is a disagreement with PDO probably in link with the methods used to compute correlation since previous authors used full correlation while we consider partial correlation to take into account the interaction between climate indexes. As long as one of the teleconnections is positively correlated with heavy and very heavy rainfall, flooding is likely to occur if it is in lower elevated area -with consequences on infrastructure, livestock and dams- and greater surface runoff for the highland of western border.

5. Conclusions

The variability and trends of nine extreme precipitation indices over the MRB using daily rainfall from 769 NOAA weather stations, which record at least 95 % of data in a yearly timescale for the period 1988–2017 are investigated in this study. The impact of the topography on the spatial structure of the extreme precipitation indices as well as the effect of warming climate on the spatial structure of the trends are also checked. The relationships between each of the seven large-scale atmospheric teleconnections and each of the precipitation's indices was also evaluated. The main findings are summarized below.

The spatial structure of the extreme's precipitation indices is strongly influenced by the topography. The highest values of the intensity and frequency indices over the Lower Mississippi are due to increase in southerly wind that bring to much moisture from the Gulf of Mexico. With the exception being for the CDD (which shows decreasing trend), the extreme precipitation exhibits in average a non-significant increasing trend over the MRB. However, PRCPTOT shows a significant increasing trend with a magnitude of 1.04 mm/year. Trend analysis of individual stations shows that, for both frequency and intensity indices, most of the significant downward (upward) trends are in areas characterized by significant warming (cooling). The reverse is observed for the CDD while wetting conditions still prevail at some station. Overall, this study help gain insights into the coupled influence of topography and moisture flux to the spatial structure of extreme precipitation indices, the impact of warming/cooling condition on the spatial trends of extreme precipitation indices. Finally, analyzing the partial correlation between extreme precipitation and large-scale teleconnections also provides more information on their regional impact on extreme precipitation indices.

However, this study has some limitations. The study does not consider human influences such as agricultural activities (Foley et al., 2014) susceptible to modify microclimate and merits investigation in future research. In addition, the interaction between different phases (positive vs positive, positive vs negative and negative vs negative) of teleconnections also need to be studied to disentangle their combine effects on extreme indices.

Nevertheless, as far as infrastructure, agriculture and vulnerable population issues are concerned, the results of this work can help decision-makers to develop and/or adjust their mitigation and adaptation policies concerning areas vulnerable to floods and drought. In addition, the present study opens up new horizons for further research into the extreme indices highlighted here.

Table 4
List of abbreviations

Abbreviations	Spelling
AMO	Atlantic Multidecadal Oscillation
AO	Artic Oscillation
PCI	Precipitation Concentration Index
MRB	Mississippi River Basin
NAO	North Atlantic Oscillation
PNA	Pacific North American
SOI	Southern Oscillation Index
PDO	Pacific Decadal Oscillation
NOAA	National Oceanic and Atmospheric Administration

CRediT authorship contribution statement

Atanas Dommo: Writing – review & editing, Writing – original draft, Software, Methodology, Investigation, Formal analysis, Data curation, Conceptualization. **Noel Aloysius:** Writing – review & editing, Supervision, Funding acquisition. **Anthony Lupo:** Writing – review & editing, Supervision. **Sherry Hunt:** Writing – review & editing, Validation.

Declaration of Competing Interest

The authors declare that they have no known competing financial interests or personal relationships that could have appeared to influence the work reported in this paper.

Data availability

the data used are available at https://www.ncei.noaa.gov/products/land-based-station/global-historical-climatology-network-daily

Acknowledgements

This research is supported by the School of Natural Resources and College of Engineering, University of Missouri startup funds to N. Aloysius, and the U.S. Department of Agriculture – Agricultural Research Service Non-Assistance Cooperative Agreement. Mention of trade names or commercial products in this publication is solely for the purpose of providing specific information and does not imply recommendation or endorsement by the U.S. Department of Agriculture. USDA is an equal opportunity provider and employer. We acknowledge the National Oceanic and Atmospheric Administration (NOAA) for freely releasing the data that supports this work. The authors also thank the three anonymous reviewers for their dedication to improving the quality of this study.

Appendix A. Supporting information

Supplementary data associated with this article can be found in the online version at doi:10.1016/j.ejrh.2024.101954.

References

Alexander, L.V., Hope, P., Collins, D., Trewin, B., Lynch, A.H., Nicholls, N., 2007. Trends in Australia's climate means and extremes: a global context. Aust. Meteorol. Mag. 1–18.

Alexandersson, H., 1986. A homogeneity test applied to precipitation data. J. Climatol. *6* (6), 661–675. https://doi.org/10.1002/joc.3370060607.

Almazroui, M., Islam, M.N., Saeed, F., Saeed, S., Ismail, M., Ehsan, M.A., Diallo, I., O'Brien, E., Ashfaq, M., Martínez-Castro, D., Cavazos, T., Cerezo-Mota, R., Tippett, M.K., Gutowski Jr., W.J., Alfaro, E.J., Hidalgo, H.G., Vichot-Llano, A., Campbell, J.D., Kamil, S., Barlow, M., 2021. Projected Changes in Temperature and Precipitation Over the United States, Central America, and the Caribbean in CMIP6 GCMs. Earth Syst. Environ. *5* (1), 1–24. https://doi.org/10.1007/s41748-021-00199-5.

Anderson, B.T., Wang, J., Salvucci, G., Gopal, S., Islam, S., 2010. Observed Trends in Summertime Precipitation over the Southwestern United States. J. Clim. *23* (7), 1937–1944. https://doi.org/10.1175/2009jcli3317.1.

Anderson, B.T., Gianotti, D.J., Salvucci, G.D., 2015. Detectability of historical trends in station-based precipitation characteristics over the continental United States. J. Geophys. Res.: Atmospheres *120* (10), 4842–4859. https://doi.org/10.1002/2014jd022960.

Balling Jr., R.C., Goodrich, G.B., 2010. Spatial analysis of variations in precipitation intensity in the USA. Theor. Appl. Climatol. *104* (3–4), 415–421. https://doi.org/10.1007/s00704-010-0353-0.

Barnston, A.G., Livezey, R.E., 1987. Classification, Seasonality and Persistence of Low-Frequency Atmospheric Circulation Patterns. Mon. Weather Rev. *115* (6), 1083–1126. https://doi.org/10.1175/1520-0493(1987)115<1083:csapol>2.0.co;2.

Benedict, I., van Heerwaarden, C.C., Weerts, A.H., Hazeleger, W., 2019. The benefits of spatial resolution increase in global simulations of the hydrological cycle evaluated for the Rhine and Mississippi basins. Hydrol. Earth Syst. Sci. *23* (3), 1779–1800. https://doi.org/10.5194/hess-23-1779-2019.

Bessaklia, H., Ghenim, A.N., Megnounif, A., Martin-Vide, J., 2018. Spatial variability of concentration and aggressiveness of precipitation in North-East of Algeria. J. Water Land Dev. *36* (1), 3–15. https://doi.org/10.2478/jwld-2018-0001.

Bishop, D.A., Williams, A.P., Seager, R., Fiore, A.M., Cook, B.I., Mankin, J.S., Singh, D., Smerdon, J.E., Rao, M.P., 2019. Investigating the Causes of Increased Twentieth-Century Fall Precipitation over the Southeastern United States. J. Clim. *32* (2), 575–590. https://doi.org/10.1175/jcli-d-18-0244.1.

Brown, P.J., Bradley, R.S., Keimig, F.T., 2010. Changes in extreme climate indices for the Northeastern United States, 1870–2005. J. Clim. *23* (24), 6555–6572. https://doi.org/10.1175/2010jcli3363.1.

Buishand, T.A., 1982. Some methods for testing the homogeneity of rainfall records. J. Hydrol. *58* (1–2), 11–27. https://doi.org/10.1016/0022-1694(82)90066-x.

Choi, G., Collins, D., Ren, G., Trewin, B., Baldi, M., Fukuda, Y., Afzaal, M., Pianmana, T., Gomboluudev, P., Huong, P.T.T., Lias, N., Kwon, W.-T., Boo, K.-O., Cha, Y.-M., Zhou, Y., 2009. Changes in means and extreme events of temperature and precipitation in the Asia-Pacific Network region, 1955-2007. Int. J. Climatol. *29* (13), 1906–1925. https://doi.org/10.1002/joc.1979.

Cullen, H.M., deMenocal, P.B., 2000. North Atlantic influence on Tigris-Euphrates streamflow. Int. J. Climatol. *20* (8), 853–863. https://doi.org/10.1002/1097-0088(20000630)20:8<853::aid-joc497>3.0.co;2-m.

Curtis, S., 2007. The Atlantic multidecadal oscillation and extreme daily precipitation over the US and Mexico during the hurricane season. Clim. Dyn. *30* (4), 343–351. https://doi.org/10.1007/s00382-007-0295-0.

van den Besselaar, E.J.M., Klein Tank, A.M.G., Buishand, T.A., 2012. Trends in European precipitation extremes over 1951-2010 (n/a-n/a). Int. J. Climatol.. https://doi.org/10.1002/joc.3619.

van der Wiel, K., Kapnick, S.B., Vecchi, G.A., Smith, J.A., Milly, P.C.D., Jia, L., 2018. 100-Year Lower Mississippi Floods in a Global Climate Model: Characteristics and Future Changes. J. Hydrometeorol. *19* (10), 1547–1563. https://doi.org/10.1175/jhm-d-18-0018.1.

Donat, M.G., Peterson, T.C., Brunet, M., King, A.D., Almazroui, M., Kolli, R.K., Boucherf, D., Al-Mulla, A.Y., Nour, A.Y., Aly, A.A., Nada, T.A.A., Semawi, M.M., Al Dashti, H.A., Salhab, T.G., El Fadli, K.I., Muftah, M.K., Dah Eida, S., Badi, W., Driouech, F., Al Shekaili, M.N., 2013. Changes in extreme temperature and precipitation in the Arab region: long-term trends and variability related to ENSO and NAO. Int. J. Climatol. *34* (3), 581–592. https://doi.org/10.1002/joc.3707.

Durkee, J.D., Frye, J.D., Fuhrmann, C.M., Lacke, M.C., Jeong, H.G., Mote, T.L., 2007. Effects of the North Atlantic Oscillation on precipitation-type frequency and distribution in the eastern United States. Theor. Appl. Climatol. *94* (1–2), 51–65. https://doi.org/10.1007/s00704-007-0345-x.

Dušek, J., Hudecová, Š., Stellner, S., 2017. Extreme precipitation and long-term precipitation changes in a Central European sedge-grass marsh in the context of flood occurrence. Hydrol. Sci. J. *62* (11), 1796–1808. https://doi.org/10.1080/02626667.2017.1353217.

Enfield, D.B., Mestas-Nuñez, A.M., Trimble, P.J., 2001. The Atlantic Multidecadal Oscillation and its relation to rainfall and river flows in the continental U.S. Geophys. Res. Lett. *28* (10), 2077–2080. https://doi.org/10.1029/2000gl012745.

Foley, J.A., Kucharik, C.J., Twine, T.E., Coe, M.T., Donner, S.D., 2004. Land use, land cover, and climate change across the Mississippi Basin: Impacts on selected land and water resources. Ecosystems and Land Use Change. American Geophysical Union, pp. 249–261.

Frich, P., Alexander, L., Della-Marta, P., Gleason, B., Haylock, M., Klein Tank, A., Peterson, T., 2002. Observed coherent changes in climatic extremes during the second half of the twentieth century. Clim. Res. *19*, 193–212. https://doi.org/10.3354/cr019193.

Gao, L., Huang, J., Chen, X., Chen, Y., Liu, M., 2018. Contributions of natural climate changes and human activities to the trend of extreme precipitation. Atmos. Res. *205*, 60–69. https://doi.org/10.1016/j.atmosres.2018.02.006.

Greatbatch, R.J., 2000. The North Atlantic Oscillation. Stoch. Environ. Res. Risk Assess. *14* (4), 0213–0242. https://doi.org/10.1007/s004770000047.
Griffiths, M.L., Bradley, R.S., 2007. Variations of Twentieth-Century Temperature and Precipitation Extreme Indicators in the Northeast United States. J. Clim. *20* (21), 5401–5417. https://doi.org/10.1175/2007jcli1594.1.
Hamed, K.H., Rao, A.Ramachandra, 1998. A modified Mann-Kendall trend test for autocorrelated data. J. Hydrol. 204, 182–196. https://doi.org/10.1016/s0022-1694(97)00125-x.
Hayhoe, K., Wuebbles, D.J., Easterling, D.R., Fahey, D.W., Doherty, S., Kossin, J.P., Sweet, W.V., Vose, R.S., Wehner, M.F., 2018. Chapter 2: Our Changing Climate. Impacts, Risks, and Adaptation in the United States: The Fourth National Climate Assessment, Volume II. U.S. Global Change Research Program. https://doi.org/10.7930/nca4.2018.ch2.
Higgins, R.W., Silva, V.B.S., Shi, W., Larson, J., 2007. Relationships between Climate Variability and Fluctuations in Daily Precipitation over the United States. J. Clim. *20* (14), 3561–3579. https://doi.org/10.1175/jcli4196.1.
Howarth, M.E., Thorncroft, C.D., Bosart, L.F., 2019. Changes in Extreme Precipitation in the Northeast United States: 1979–2014. J. Hydrometeorol. *20* (4), 673–689. https://doi.org/10.1175/jhm-d-18-0155.1.
Huang, H., Winter, J.M., Osterberg, E.C., Horton, R.M., Beckage, B., 2017. Total and Extreme Precipitation Changes over the Northeastern United States. J. Hydrometeorol. 18, 1783–1798. https://doi.org/10.1175/jhm-d-16-0195.1.
Hurrell, J.W., 1995. Decadal Trends in the North Atlantic Oscillation: Regional Temperatures and Precipitation. Science *269* (5224), 676–679. https://doi.org/10.1126/science.269.5224.676.
Hurrell, J.W., Dickson, R.R., 2005. Climate Variability Over the North Atlantic. Marine Ecosystems and Climate Variation. Oxford University PressOxford, pp. 15–32. https://doi.org/10.1093/acprof:oso/9780198507499.003.0002.
Karl, T.R., Knight, R.W., 1998. Secular Trends of Precipitation Amount, Frequency, and Intensity in the United States. Bull. Am. Meteorol. Soc. 79, 231–241. https://doi.org/10.1175/1520-0477(1998)079<0231:stopaf>2.0.co;2.
Karl, T.R., Knight, R.W., Easterling, D.R., Quayle, R.G., 1996. Indices of Climate Change for the United States. Bull. Am. Meteorol. Soc. *77* (2), 279–292. https://doi.org/10.1175/1520-0477(1996)077<0279:IOCCFT>2.0.CO;2.
Katz, R.W., Brown, B.G., 1992. Extreme events in a changing climate: Variability is more important than averages. Clim. Change 21, 289–302. https://doi.org/10.1007/bf00139728.
Kendall, M.G., 1955. Further Contributions to the Theory of Paired Comparisons. Biometrics *11* (1), 43. https://doi.org/10.2307/3001479.
Kesel, R.H., Schaetzl, R.J., & Severin, G.T. (1998). Mississippi River. In *Encyclopedia Britannica*. ⟨https://www.britannica.com/place/Mississippi-River⟩.
Khaliq, M.N., Ouarda, T.B.M.J., Ondo, J.-C., Gachon, P., Bobée, B., 2006. Frequency analysis of a sequence of dependent and/or non-stationary hydro-meteorological observations: A review. J. Hydrol. 329, 534–552. https://doi.org/10.1016/j.jhydrol.2006.03.004.
Klein Tank, A.M.G., Können, G.P., 2003. Trends in Indices of Daily Temperature and Precipitation Extremes in Europe, 1946–99. J. Clim. *16* (22), 3665–3680. https://doi.org/10.1175/1520-0442(2003)016<3665:tiiodt>2.0.co;2.
Klein Tank, A.M.G., Wijngaard, J.B., Können, G.P., Böhm, R., Demarée, G., Gocheva, A., Mileta, M., Pashiardis, S., Hejkrlik, L., Kern-Hansen, C., Heino, R., Bessemoulin, P., Müller-Westermeier, G., Tzanakou, M., Szalai, S., Pálsdóttir, T., Fitzgerald, D., Rubin, S., Capaldo, M., Petrovic, P., 2002. Daily dataset of 20th-century surface air temperature and precipitation series for the European Climate Assessment. Int. J. Climatol. *22* (12), 1441–1453. https://doi.org/10.1002/joc.773.
Kunkel, K.E., Andsager, K., Easterling, D.R., 1999. Long-Term Trends in Extreme Precipitation Events over the Conterminous United States and Canada. J. Clim. 12, 2515–2527. https://doi.org/10.1175/1520-0442(1999)012<2515:lttiep>2.0.co;2.
Latif, Y., Ma, Y., Ma, W., 2021. Climatic trends variability and concerning flow regime of Upper Indus Basin, Jehlum, and Kabul River basins Pakistan. Theor. Appl. Climatol. *144* (1–2), 447–468. https://doi.org/10.1007/s00704-021-03529-9.
Lebedeva, M.G., Lupo, A.R., Chendev, Y.G., Krymskaya, O.V., Solovyev, A.B., 2019. Changes in the Atmospheric Circulation Conditions and Regional Climatic Characteristics in Two Remote Regions Since the Mid-20th Century. Atmosphere *10* (1), 11. https://doi.org/10.3390/atmos10010011.
Li, F., Ju, X., Lu, W., Li, H., 2019. A comprehensive analysis of spatial and temporal variability of extreme precipitation in the Nenjiang River Basin, Northeast China. Theor. Appl. Climatol. *138* (1–2), 605–616. https://doi.org/10.1007/s00704-019-02846-4.
Li, X., Wang, X., Babovic, V., 2017. Analysis of variability and trends of precipitation extremes in Singapore during 1980-2013. Int. J. Climatol. *38* (1), 125–141. https://doi.org/10.1002/joc.5165.
van Loon, H., Rogers, J.C., 1978. The Seesaw in Winter Temperatures between Greenland and Northern Europe. Part I: General Description. Mon. Weather Rev. *106* (3), 296–310. https://doi.org/10.1175/1520-0493(1978)106<0296:tsiwtb>2.0.co;2.
de Luis, M., González-Hidalgo, J.C., Brunetti, M., Longares, L.A., 2011. Precipitation concentration changes in Spain 1946–2005. Nat. Hazards Earth Syst. Sci. *11* (5), 1259–1265. https://doi.org/10.5194/nhess-11-1259-2011.
Mallakpour, I., Villarini, G., 2016. Analysis of changes in the magnitude, frequency, and seasonality of heavy precipitation over the contiguous USA. Theor. Appl. Climatol. *130* (1–2), 345–363. https://doi.org/10.1007/s00704-016-1881-z.
Mann, H.B., 1945. Nonparametric tests against trend. Econometrica *13* (3), 245. https://doi.org/10.2307/1907187.
Mantua, N., Tohver, I., Hamlet, A., 2010. Climate change impacts on streamflow extremes and summertime stream temperature and their possible consequences for freshwater salmon habitat in Washington State. Clim. Change 102, 187–223. https://doi.org/10.1007/s10584-010-9845-2.
Mantua, N.J., Hare, S.R., Zhang, Y., Wallace, J.M., Francis, R.C., 1997. A Pacific Interdecadal Climate Oscillation with Impacts on Salmon Production. Bull. Am. Meteorol. Soc. *78* (6), 1069–1079. https://doi.org/10.1175/1520-0477(1997)078<1069:apicow>2.0.co;2.
Maurer, E.P., Lettenmaier, D.P., 2003. Predictability of seasonal runoff in the Mississippi River basin. J. Geophys. Res.: Atmospheres 108. https://doi.org/10.1029/2002jd002555.
Mearns, L.O., Katz, R.W., Schneider, S.H., 1984. Extreme High-Temperature Events: Changes in their probabilities with Changes in Mean Temperature. J. Clim. Appl. Meteorol. 23, 1601–1613. https://doi.org/10.1175/1520-0450(1984)023<1601:ehteci>2.0.co;2.
Menne, M.J., Durre, I., Vose, R.S., Gleason, B.E., Houston, T.G., 2012. An Overview of the Global Historical Climatology Network-Daily Database. J. Atmos. Ocean. Technol. *29* (7), 897–910. https://doi.org/10.1175/jtech-d-11-00103.1.
Nigam, S., Sengupta, A., 2021. The Full Extent of El Niño's Precipitation Influence on the United States and the Americas: The Suboptimality of the Niño 3.4 SST Index. Geophys. Res. Lett. *48* (3) https://doi.org/10.1029/2020gl091447.
Oliver, J.E., 1980. MONTHLY PRECIPITATION DISTRIBUTION: A COMPARATIVE INDEX. Prof. Geogr. *32* (3), 300–309. https://doi.org/10.1111/j.0033-0124.1980.00300.x.
Peterson, T.C., Folland, C., Gruza, G., Hogg, W., Mokssit, A., & Plummer, N. (2001). *Report on the Activities of the Working Group on Climate Change Detection and Related Rapporteurs, 1998-2001*.
Peterson, T.C., Heim Jr., R.R., Hirsch, R., Kaiser, D.P., Brooks, H., Diffenbaugh, N.S., Dole, R.M., Giovannettone, J.P., Guirguis, K., Karl, T.R., Katz, R.W., Kunkel, K., Lettenmaier, D., McCabe, G.J., Paciorek, C.J., Ryberg, K.R., Schubert, S., Silva, V.B.S., Stewart, B.C., Wuebbles, D., 2013. Monitoring and Understanding Changes in Heat Waves, Cold Waves, Floods, and Droughts in the United States: State of Knowledge. Bull. Am. Meteorol. Soc. *94* (6), 821–834. https://doi.org/10.1175/bams-d-12-00066.1.
Pettitt, A.N., 1979. A non-parametric approach to the change-point problem. Appl. Stat. *28* (2), 126. https://doi.org/10.2307/2346729.
Quan, N.T., Khoi, D.N., Hoan, N.X., Phung, N.K., Dang, T.D., 2020. Spatiotemporal Trend Analysis of Precipitation Extremes in Ho Chi Minh City, Vietnam During 1980–2017. Int. J. Disaster Risk Sci. *12* (1), 131–146. https://doi.org/10.1007/s13753-020-00311-9.
Rayner, N.A., Parker, D.E., Horton, E.B., Folland, C.K., Alexander, L.V., Rowell, D.P., Kent, E.C., Kaplan, A., 2003. Global analyses of sea surface temperature, sea ice, and night marine air temperature since the late nineteenth century. J. Geophys. Res.: Atmospheres *108* (D14). https://doi.org/10.1029/2002jd002670.
Ropelewski, C.F., Jones, P.D., 1987. An Extension of the Tahiti–Darwin Southern Oscillation Index. Mon. Weather Rev. *115* (9), 2161–2165. https://doi.org/10.1175/1520-0493(1987)115<2161:aeotts>2.0.co;2.

Rosenzweig, C., Tubiello, F.N., Goldberg, R., Mills, E., Bloomfield, J., 2002. Increased crop damage in the US from excess precipitation under climate change. Glob. Environ. Change *12* (3), 197–202. https://doi.org/10.1016/s0959-3780(02)00008-0.

Sen, P.K., 1968. Estimates of the regression coefficient based on Kendall's tau. J. Am. Stat. Assoc. 63, 1379–1389.

Shawul, A.A., Chakma, S., 2020. Trend of extreme precipitation indices and analysis of long-term climate variability in the Upper Awash basin, Ethiopia. Theor. Appl. Climatol. *140* (1–2), 635–652. https://doi.org/10.1007/s00704-020-03112-8.

Sheikh, M.M., Manzoor, N., Ashraf, J., Adnan, M., Collins, D., Hameed, S., Manton, M.J., Ahmed, A.U., Baidya, S.K., Borgaonkar, H.P., Islam, N., Jayasinghearachchi, D., Kothawale, D.R., Premalal, K.H.M.S., Revadekar, J.V., Shrestha, M.L., 2014. Trends in extreme daily rainfall and temperature indices over South Asia. Int. J. Climatol. *35* (7), 1625–1637. https://doi.org/10.1002/joc.4081.

Shenoy, S., Gorinevsky, D., Trenberth, K.E., Chu, S., 2022. Trends of extreme US weather events in the changing climate. Proc. Natl. Acad. Sci. *119* (47) https://doi.org/10.1073/pnas.2207536119.

Smith, J.A., Baeck, M.L., 2015. "Prophetic vision, vivid imagination": The 1927 M ississippi R iver flood. Water Resour. Res. *51* (12), 9964–9994. https://doi.org/10.1002/2015wr017927.

Smithson, P.A., 2002. IPCC, 2001: climate change 2001: the scientific basis. Contribution of Working Group 1 to the Third Assessment Report of the Intergovernmental Panel on Climate Change, edited by J. T. Houghton, Y. Ding, D. J. Griggs, M. Noguer, P. J. van der Linden, X. Da, 1144–1144 Int. J. Climatol. *22* (9). https://doi.org/10.1002/joc.763.

Sutton, R.T., Hodson, D.L.R., 2005. Atlantic Ocean Forcing of North American and European Summer Climate. Science *309* (5731), 115–118. https://doi.org/10.1126/science.1109496.

Thompson, D.W.J., Wallace, J.M., 1998. The Arctic oscillation signature in the wintertime geopotential height and temperature fields. Geophys. Res. Lett. *25* (9), 1297–1300. https://doi.org/10.1029/98gl00950.

Thompson, D.W.J., Wallace, J.M., 2001. Regional Climate Impacts of the Northern Hemisphere Annular Mode. Science *293* (5527), 85–89. https://doi.org/10.1126/science.1058958.

Tian, J., Liu, J., Wang, J., Li, C., Nie, H., Yu, F., 2016. Trend analysis of temperature and precipitation extremes in major grain producing area of China. Int. J. Climatol. *37* (2), 672–687. https://doi.org/10.1002/joc.4732.

Toreti, A., Desiato, F., 2008. Changes in temperature extremes over Italy in the last 44 years. Int. J. Climatol. *28* (6), 733–745. https://doi.org/10.1002/joc.1576.

Trenberth, K.E., Dai, A., Rasmussen, R.M., Parsons, D.B., 2003. The Changing Character of Precipitation. Bull. Am. Meteorol. Soc. *84* (9), 1205–1218. https://doi.org/10.1175/bams-84-9-1205.

Wahl, K.L., Vining, K.C., Wiche, G.J., 1993. Precipitation in the upper Mississippi River basin, January 1 through July 31, 1993. Circular. https://doi.org/10.3133/cir1120b.

Wang, J., 2013. Partial correlation coefficient. Encyclopedia of Systems Biology. Springer, New York, pp. 1634–1635.

Xiong, K.-G., Feng, G.L., Qiguang, W., Hu, J.-G., 2009. Acta Phys. Sin. *58* (11), 8107–8115. https://doi.org/10.77498/aps.58.8107.

Yin, J., Yan, D., Yang, Z., Yuan, Z., Yuan, Y., Zhang, C., 2016. Projection of extreme precipitation in the context of climate change in Huang-Huai-Hai region, China. J. Earth Syst. Sci. *125* (2), 417–429. https://doi.org/10.1007/s12040-016-0664-3.

Zamani, R., Mirabbasi, R., Nazeri, M., Meshram, S.G., Ahmadi, F., 2017. Spatio-temporal analysis of daily, seasonal and annual precipitation concentration in Jharkhand state, India. Stoch. Environ. Res. Risk Assess. *32* (4), 1085–1097. https://doi.org/10.1007/s00477-017-1447-3.

Zhang, K., Yao, Y., Qian, X., Wang, J., 2019. Various characteristics of precipitation concentration index and its cause analysis in China between 1960 and 2016. Int. J. Climatol. *39* (12), 4648–4658. https://doi.org/10.1002/joc.6092.

Zhang, Q., Xu, C.-Y., Tao, H., Jiang, T., Chen, Y.D., 2009. Climate changes and their impacts on water resources in the arid regions: a case study of the Tarim River basin, China. Stoch. Environ. Res. Risk Assess. *24* (3), 349–358. https://doi.org/10.1007/s00477-009-0324-0.

Zhang, X., Alexander, L., Hegerl, G.C., Jones, P., Tank, A.K., Peterson, T.C., Trewin, B., Zwiers, F.W., 2011. Indices for monitoring changes in extremes based on daily temperature and precipitation data. WIREs Clim. Change *2* (6), 851–870. https://doi.org/10.1002/wcc.147.

Zhang, Y., Wallace, J.M., Battisti, D.S., 1997. ENSO-like Interdecadal Variability: 1900–93. J. Clim. *10* (5), 1004–1020. https://doi.org/10.1175/1520-0442(1997)010<1004:eliv>2.0.co;2.